Arch Appl Mech
DOI 10.1007/s00419-017-1259-4

SPECIAL

Stefan Hartmann · Rose Rogin Gilbert

Identifiability of material parameters in solid mechanics

Received: 6 November 2016 / Accepted: 27 April 2017

Abstract Material parameter identification using constitutive models of elasticity, viscoelasticity, rate-independent plasticity and viscoplasticity has a long history with regard to homogeneous and inhomogeneous deformations. For example, uniaxial tensile tests, pure shear tests, torsion experiments of thin-walled tubes or biaxial tensile tests are used to obtain the material parameters by solving the inverse problem. Frequently, the parameters are determined by numerical optimization tools. In this paper, we investigate some very basic single- and two-layered examples regarding identifiability, because these tests are the basis for more complex geometrical and physical nonlinear problems. These simple examples are the uniaxial tensile/compression case, biaxial tensile tests of a cruciform specimen, torsion of a thin-walled tube, a thick-walled tube under internal pressure and the indentation test. For the thick-walled tube under internal and external pressure with an axial pre-strain with several layers, an analytical solution is provided directly suitable for programming. The aim is to get an understanding whether some problems lead to non-identifiable parameters.

Keywords Identifiability · Material parameter identification · Thick-walled tube · Multi-layered materials · Indentation · Sensitivity analysis · Finite element method

1 Introduction

In the field of solid mechanics, there exist a huge amount of constitutive models, due to the fact that there are a diversity of materials and a variety of physical observations under particular loading paths. All these models have material parameters, which have to be calibrated to the experimental data in order to describe the material behavior in a certain range of application. This calibration is called *material parameter identification* or briefly *parameter identification*.

There are different proposals for constitutive models that represent the relation between the strain history and the current stress state, see, for example, [33,48,50,77]. These models are formulated as algebraic equations in the case of elasticity, ordinary differential equations or integral equations for models of viscoelasticity, rate-independent plasticity or viscoplasticity. Extensions might also be partial differential equations to incorporate size-dependent effects or non-local properties of the material, see [38,55], as well as FE^2-methods, where several constituents in a representative volume element define the overall material behavior, [67,68], to incorporate local material properties, i.e., models where we have to determine the "local material parameters." Moreover, coupled problems have to be incorporated as well, as they occur in, for instance, thermomechanical, electromechanical, magnetomechanical fields simulations.

S. Hartmann (✉) · R. R. Gilbert
Institute of Applied Mechanics, Clausthal University of Technology, Adolph-Roemer-Str. 2a, 38678 Clausthal-Zellerfeld, Germany
E-mail: stefan.hartmann@tu-clausthal.de
Tel.: +49-5323-722774

Published online: 08 May 2017

In the following, we restrict ourselves to the simplest models, but some basic problems in the parameter estimation process might occur even in this case. Commonly, models are proposed for one-dimensional stress–strain relations in the development phase of constitutive modeling. In a second phase, these one-dimensional models (stress–strain functionals) are extended to a three-dimensional formulation using tensorial stress–strain relations, which are accompanied by additional equations for internal variables, in view of the theory of internal variables, see [15]. However, the material parameters of the three-dimensional models are equivalent to the one-dimensional counterpart only in very special situations. Thus, three-dimensional considerations are required.

Frequently, uniaxial tensile tests are carried out in order to obtain a specified, homogeneously distributed stress and homogeneously distributed strain state within a small region of the specimen. This is possible for small and finite deformations. Compression tests, however, are more difficult, since the specimens might exhibit buckling effects, e.g., in the case of foils, or bulging for elastomeric specimens, see, for instance, [1,30]. In other words, the stress and strain state is determined in a small region of a specimen up to a certain limit of deformation. Tensile specimens with notches are mainly chosen to determine the ductility of the material, see [19], since there is no specified strain and stress state within the thinner region. Of course, the local strain distribution can be measured by a DIC-system, which, however, is very sensitive in the center of the notch.

Alternatively, torsion tests of thin-walled tubes can be used for the small-strain case. Under the assumption of a constant shear stress over the thickness of the tube's wall, it is possible to obtain a homogeneously distributed shear stress and shear strain state, see [34] and the references cited therein. The aim of reaching large deformations under torsion is restricted by buckling in the case of thin-walled structures. However, torsion tests for the case of large strains can be performed using cylindrical specimens with full cross section. Haupt and Sedlan [35] provided such experiments using specimens with circular cross section, where the assumption of isotropy and incompressibility is considered, see [39] as well. However, this is an inhomogeneous deformation state. In this case—since the stress state is spatially not constant—the resulting torque and the normal (axial) force are chosen to identify the parameters as integral quantities.

The shear of thin metal sheets or polymer foils is a further possibility to obtain insight into the material behavior for the case of small deformations. For large strains, this is questionable since there are inhomogeneous deformations at the edges, and, accordingly, the stress state cannot be specified. Furthermore, buckling might occur beyond a certain deformation state. The deformation state can be obtained by geometrical assumptions in the case of small strains, or, in the case of large strains, by optical full-field measurement systems such as digital image correlation (DIC), see, for example, [72]. On the one hand, there might be normal stresses introduced in the specimen, and, on the other hand, the shear stresses cannot be determined by shear force divided by cross section because the cross section is not really clear due to boundary effects.

Biaxial tensile tests are a common trend since they are attractive for full-field measurement systems, see [21,72]. Only the strain state can be determined by these digital imaging correlation systems. However, the stress state is undetermined (what is the cross section in the middle region of the cruciform specimens?). Accordingly, it is only possible to measure the resulting forces as an integral quantity. Thus, experiments, for which no specified stress–strain state is provided, can only be used for validation purposes, to determine the limits in multiaxial stress–strain states, or to calibrate an existing model.

More complicated tasks are three-dimensional tensile and compression tests, see [11,70], since there is no optical access to the specimens. Further, they are difficult to produce, and the stress state is undetermined. Even in these cases, it is only possible to measure integral quantities, namely the reaction forces.

Three- and four-point flexural (bending) tests can be chosen to determine the deformation (deflection) at one point in dependence of a given external force. However, only Young's modulus is being sought for. For particular materials and small size, the three-dimensional deformation can be measured, see [24]. Of course, DIC can be chosen at the lateral surface of the beam as well. It will turn out that the Poisson number is not determinable.

The case of thick-walled tubes under internal pressure provides information regarding the axial forces (caused by the material's property of showing a lateral deformation to its loading direction, which here is fixed, and, as a consequence, yields an axial force) and the outer surface deformation (either the radial displacements, see [8], or the circumferential strains using, for instance, strain gauges). The major problems in experiments are to be seen in safety considerations in case the internal pressure exceeds a certain limit, as well as in the small deformations on the outer surface for small-strain applications. Possible large deformation applications are, for instance, biomechanical applications of inflated arteries, see [26]. In the latter case, however, additional inhomogeneous deformations will occur at the boundaries where the arteries are fixed. Moreover, they do not represent ideal axisymmetric cylinders.

Indentation tests are used as well in order to determine parameters for constitutive models. However, we obtain only force and indentation depth behavior in this case, which are, again, integral quantities. Furthermore, the relation to constitutive modeling can only be seen as an indicator. In this respect, and with regard to identification, see, for example, [13,36,37,45,61].

The simplest approach to determine the parameters is to search manually in order to approximately reproduce the material behavior. This can be done if models are very simple or if most of the parameters are known and only one parameter has to be varied. Alternatively, optimization algorithms can be applied, see, for example, [22,44] for linear problems or [4,20,51,56] for nonlinear problems with and without equality and inequality constraints. In this case, numerical tools serve to determine the minimum of residual between the mathematical model and the experimental data.

The optimization tools can be applied either to the one-dimensional model equations yielding a linear or nonlinear least-square problem, see, for details, [5,74], or to the entire solution of the boundary value problem. There are a number of difficulties that might occur. First, if a model is slightly more complex and the experimental data are limited, i.e., the data do not address some of the parameters, the obtained parameters might, however, not make any sense regarding their physical meaning. One approach to circumvent this problem is the stepwise identification of the parameters and/or the application of constitutive models which have a certain modular structure such as overstress-type models, see [34,49] and the literature cited therein. Although this is a helpful approach, it does not necessarily yield reliable identified material parameters. A further difficulty might arise if three-dimensional models have to be reduced to the uniaxial tensile case due to the assumption of a stress-free boundary condition in lateral direction.

In this context, a linear least-square problem is discussed in [28,29] for the case of hyperelasticity showing that the identification might lead to highly sensitive parameters so that results of a parameter with all digits are important. Furthermore, no further information concerning the physical meaning of polynomial-based approaches of the strain energy functions is provided. The nonlinear case is given by Ogden-type models, see [78], where similar problems are observed.

If the constitutive equations are of rate type, i.e., there are further evolution equations for internal variables, we refer to [40] and the literature cited therein. In this case, the entire constitutive model, in its three-dimensional formulation, is used for parameter estimation purposes. Here, solvers for ordinary differential or differential–algebraic equations have to be applied. This leads to further challenging aspects, see [64] in view of highly accurate time integration schemes.

If the underlying experiments yield inhomogeneous stress or strain fields, the optimization tool, which has to compute the residuum of the simulation and the experimental data, requires the solution of an entire initial boundary value problem. Commonly, the finite element method is chosen (if there is no analytic solution, which is commonly the case). In this respect, we refer to [2,52,53], where it was Mahnken who mainly shaped this kind of identification procedure. In later contributions of [6,41,42,63] also finite elements are used in the parameter identification process. Additionally, we would like to refer to [30,31] as well as [13,36,37,45,61]. In view of micro-mechanical modeling, we refer to [67,68].

As stated in Schittkowski [64], the numerical solution of ordinary differential equations and differential–algebraic equations can have an influence on the result of the identification or might lead to problems if numerical differentiation is applied in gradient-based optimization methods. This statement can be extended to spatial discretization schemes such as the finite element method as well. However, a systematic investigation is still an open issue—and this aspect will not be addressed in the scope of this publications.

Apart from both the experimental problems of providing sufficient data with less noise as well as the aforementioned numerical problems caused by inaccurate computations, there are further principal problems in the identification process. For example, it is still not yet possible to determine the material parameters of an artery (consisting of two contributing layers, adventitia and media) in an uncorrelated manner, see, for example, [26]. Each layer might be modeled by another hyperelasticity relation. This problem leads back to a basic question, namely under which circumstances the material parameters are identifiable. This idea goes back to Beveridge and Schechter [7], see [5] as well. The approach has been applied by [69] for structural dynamic problems later on. In [5,7], a quadratic approximation of the objective function is evaluated in the minimum, which is computed beforehand. The evaluation of the Hessian at the local minimum is applied for various experiments with the simplest models. It will be shown what kind of difficulties might arise even for the simple models. Furthermore, it is applied to one- and two-layered materials. We start to treat the uniaxial tensile case and apply a three-dimensional model in different representations. Here, we restrict ourselves to a small-strain, linear isotropic case. Even this case shows basic problems, which have to be addressed in the

identification process. Afterward, we extend these investigations to biaxial tension, the thick-walled tube under internal pressure, and later on to an indentation test.

The notation in use is defined in the following manner: geometrical vectors are symbolized by $\mathbf{a}$, second-order tensors $\mathbf{A}$ by bold-faced Roman letters, and calligraphic letters $\mathcal{A}$ define fourth-order tensors. Furthermore, we introduce matrices symbolized by bold-faced italic letters $\boldsymbol{A}$.

2 Least-square problem

We start with the least-square problem, which is frequently the basis of the parameter estimation process. The square of the norm of the residuum $\boldsymbol{r}(\boldsymbol{\kappa}) = \boldsymbol{s}(\boldsymbol{\kappa}) - \boldsymbol{d}$ between the model $\boldsymbol{s} \in \mathbb{R}^{n_\mathrm{d}}$—we call it simulation data—and the experimental data $\boldsymbol{d} \in \mathbb{R}^{n_\mathrm{d}}$ should reach a minimum, which is a common approach. If the experimental data and the simulation data are not evaluated at the same time, linear interpolation has to be performed, where we apply this to the simulation data, if necessary. The simulation depends on the material parameters $\boldsymbol{\kappa} \in \mathbb{R}^{n_\kappa}$, so that the objective functions reads

$$f(\boldsymbol{\kappa}) = \frac{1}{2}\|\boldsymbol{r}(\boldsymbol{\kappa})\|^2 = \frac{1}{2}\boldsymbol{r}^T(\boldsymbol{\kappa})\boldsymbol{r}(\boldsymbol{\kappa}) = \frac{1}{2}\sum_{i=1}^{n_\mathrm{d}}(s_i(\boldsymbol{\kappa}) - d_i)^2 \quad \rightarrow \quad \min \tag{1}$$

under the inequality constraints

$$\kappa_{\min j} \leq \kappa_j \leq \kappa_{\max j}, \quad j = 1, \ldots, n_\kappa, \tag{2}$$

(the factor $1/2$ does not change the problem and is chosen for minimizing the following calculations). This requires prior knowledge about the properties of the parameters. Sometimes, particularly for models with internal variables, this is not available. For practical reasons, all parameters are assigned with constraints that can essentially stabilize the identification process (this is not essential in this article). In the linear least-square problem, we have $\boldsymbol{s}(\boldsymbol{\kappa}) = \boldsymbol{A}\boldsymbol{\kappa}$ with $\boldsymbol{A} \in \mathbb{R}^{n_\mathrm{d} \times n_\kappa}$, i.e., the simulation depends linearly on the parameters and the goal function reads

$$f(\boldsymbol{\kappa}) = \frac{1}{2}\|\boldsymbol{A}\boldsymbol{\kappa} - \boldsymbol{d}\|^2 = \frac{1}{2}\left(\boldsymbol{\kappa}^T\boldsymbol{A}^T\boldsymbol{A}\boldsymbol{\kappa} - 2\boldsymbol{\kappa}^T\boldsymbol{A}^T\boldsymbol{d} + \boldsymbol{d}^T\boldsymbol{d}\right) \quad \rightarrow \quad \min. \tag{3}$$

The necessary conditions of a minimum in Eq. (1) can be obtained by applying the Gâteaux derivative

$$\mathrm{D}\, f(\boldsymbol{\kappa})[\boldsymbol{h}] = \frac{\mathrm{d}}{\mathrm{d}\lambda} f(\boldsymbol{\kappa} + \lambda\boldsymbol{h})\Big|_{\lambda=0} = \left\{\frac{\mathrm{d}f}{\mathrm{d}\boldsymbol{\kappa}}\right\}^T \boldsymbol{h} = \sum_{k=1}^{n_\kappa} \frac{\partial f}{\partial \kappa_k} h_k = 0, \tag{4}$$

i.e., we have

$$\left.\frac{\mathrm{d}f(\boldsymbol{\kappa})}{\mathrm{d}\boldsymbol{\kappa}}\right|_{\boldsymbol{\kappa}=\boldsymbol{\kappa}^*} = \boldsymbol{0} \tag{5}$$

at the minimum $\boldsymbol{\kappa}^*$. In the linear least-square problem, this leads to

$$\mathrm{D}\, f(\boldsymbol{\kappa})[\boldsymbol{h}] = \boldsymbol{h}^T\boldsymbol{A}^T\{\boldsymbol{A}\boldsymbol{\kappa} - \boldsymbol{d}\} = \boldsymbol{h}^T \underbrace{\left\{\left[\boldsymbol{A}^T\boldsymbol{A}\right]\boldsymbol{\kappa} - \boldsymbol{A}^T\boldsymbol{d}\right\}}_{\mathrm{d}f(\boldsymbol{\kappa})/\mathrm{d}\boldsymbol{\kappa}} = 0, \tag{6}$$

i.e., for arbitrary directions $\boldsymbol{h}$, the system of linear equations

$$\left[\boldsymbol{A}^T\boldsymbol{A}\right]\boldsymbol{\kappa} = \boldsymbol{A}^T\boldsymbol{d}, \tag{7}$$

has to hold, see, for example, [5,44]. A small extension is related to weight the residual by a weighting matrix $\boldsymbol{W} \in \mathbb{R}^{n_\mathrm{d} \times n_\mathrm{d}}$ (commonly, a diagonal matrix), i.e., $\tilde{\boldsymbol{r}} = \boldsymbol{W}\boldsymbol{r}$. This weighting matrix can be chosen to weight directly only a few discrete points, to normalize different tests by their different magnitude, to equilibrate different number of test data of partial tests, or to obtain the same physical dimension, see [28]. Since this has no direct influence on the subsequent investigations, we omit these considerations.

For the nonlinear least-square problem, Eq. (1) yields

$$\mathrm{D}\, f(\boldsymbol{\kappa})[\boldsymbol{h}] = \boldsymbol{h}^T \left[\frac{\mathrm{d}\boldsymbol{s}(\boldsymbol{\kappa})}{\mathrm{d}\boldsymbol{\kappa}}\right]^T \{\boldsymbol{s}(\boldsymbol{\kappa}) - \boldsymbol{d}\} = 0, \tag{8}$$

i.e., for arbitrary $\boldsymbol{h}$ we have the system of nonlinear equations (necessary condition of a local minimum)

$$\left.\frac{\mathrm{d}f(\boldsymbol{\kappa})}{\mathrm{d}\boldsymbol{\kappa}}\right|_{\boldsymbol{\kappa}=\boldsymbol{\kappa}^*} = \boldsymbol{J}^T(\boldsymbol{\kappa}^*)\{\boldsymbol{s}(\boldsymbol{\kappa}^*) - \boldsymbol{d}\} = \boldsymbol{0}. \tag{9}$$

Here, we abbreviate the Jacobian $\boldsymbol{J}(\boldsymbol{\kappa}) := \mathrm{d}\boldsymbol{r}(\boldsymbol{\kappa})/\mathrm{d}\boldsymbol{\kappa} = \mathrm{d}\boldsymbol{s}(\boldsymbol{\kappa})/\mathrm{d}\boldsymbol{\kappa}$, $\boldsymbol{J} \in \mathbb{R}^{n_\mathrm{d} \times n_\kappa}$, where expression (9) has to vanish in a local minimum $\boldsymbol{\kappa}^*$. Commonly, the R^2-value is the first choice to specify the quality of a identification,

$$R^2 = 1 - \frac{\sum_{i=1}^{n_\mathrm{d}} (d_i - s_i)^2}{\sum_{i=1}^{n_\mathrm{d}} (d_i - \overline{d})^2}, \quad \text{with } \overline{d} = \frac{1}{n_\mathrm{d}} \sum_{i=1}^{n_\mathrm{d}} d_i, \tag{10}$$

$0 \leq R^2 \leq 1$. If $R^2 \approx 1$, we have a very good fit.

There are a number of numerical methods to solve this problem, see, for example, [4,9,20,56]. We make use of the MATLAB routines `lsqnonlin.m`, which is a trust-region-reflective algorithm. Additional issues are a nearly singular matrix $\boldsymbol{J}^T\boldsymbol{J} = \boldsymbol{A}^T\boldsymbol{A}$ in the linear optimization case leading to highly sensitive results, see discussion in [28] for hyperelasticity, which can be treated by singular value decomposition techniques, or by drawing on regularization techniques, see, for instance [75]. Furthermore, if the numerical scheme provides a solution, the quality of identification has to be investigated. In [40,42,61], the correlation matrix is called on to obtain further insight into the quality of identification. In the nonlinear case, we have two possibilities. One possibility is to apply a Taylor expansion of the residual at the solution $\boldsymbol{\kappa}^*$

$$\boldsymbol{r}(\boldsymbol{\kappa}) = \boldsymbol{r}(\boldsymbol{\kappa}^*) + \left.\frac{\mathrm{d}\boldsymbol{r}}{\mathrm{d}\boldsymbol{\kappa}}\right|_{\boldsymbol{\kappa}=\boldsymbol{\kappa}^*} \left\{\boldsymbol{\kappa} - \boldsymbol{\kappa}^*\right\} = \boldsymbol{r}(\boldsymbol{\kappa}^*) + \boldsymbol{J}(\boldsymbol{\kappa}^*)\left\{\boldsymbol{\kappa} - \boldsymbol{\kappa}^*\right\}, \tag{11}$$

leading to the linear optimization problem

$$f(\boldsymbol{\kappa}) = \frac{1}{2} \| \boldsymbol{r}(\boldsymbol{\kappa}^*) + \boldsymbol{J}(\boldsymbol{\kappa}^*)\left\{\boldsymbol{\kappa} - \boldsymbol{\kappa}^*\right\} \|, \tag{12}$$

see [9] as well, and to the computation of the covariance matrix

$$\boldsymbol{P} = s^2 \left[\boldsymbol{J}^T(\boldsymbol{\kappa}^*)\boldsymbol{J}(\boldsymbol{\kappa}^*)\right]^{-1}, \tag{13}$$

with the standard deviation

$$s^2 = \frac{1}{n_\mathrm{d} - 1} \boldsymbol{r}^T(\boldsymbol{\kappa}^*)\boldsymbol{r}(\boldsymbol{\kappa}^*). \tag{14}$$

The other approach is to approximate the objective function by a quadratic function

$$\hat{f}(\boldsymbol{\kappa}) = f(\boldsymbol{\kappa}^*) + \left\{\frac{\mathrm{d}f(\boldsymbol{\kappa})}{\mathrm{d}\boldsymbol{\kappa}}\right\}^T \Bigg|_{\boldsymbol{\kappa}=\boldsymbol{\kappa}^*} \Delta\boldsymbol{\kappa} + \frac{1}{2}\Delta\boldsymbol{\kappa}^T \left[\frac{\mathrm{d}^2 f(\boldsymbol{\kappa})}{\mathrm{d}\boldsymbol{\kappa}\mathrm{d}\boldsymbol{\kappa}}\right]\Bigg|_{\boldsymbol{\kappa}=\boldsymbol{\kappa}^*} \Delta\boldsymbol{\kappa}, \tag{15}$$

$\Delta\boldsymbol{\kappa} = \boldsymbol{\kappa} - \boldsymbol{\kappa}^*$, where the covariance matrix reads

$$\boldsymbol{P} = s^2 \boldsymbol{H}^{-1}(\boldsymbol{\kappa}^*), \tag{16}$$

with the Hessian

$$\boldsymbol{H}(\boldsymbol{\kappa}) = \frac{\mathrm{d}^2 f(\boldsymbol{\kappa})}{\mathrm{d}\boldsymbol{\kappa}\mathrm{d}\boldsymbol{\kappa}} = \left[\frac{\partial^2 f(\boldsymbol{\kappa})}{\partial\kappa_i \partial\kappa_j}\right] = \left[\sum_{k=1}^{n_\mathrm{d}} \left(\frac{\partial^2 s_k(\boldsymbol{\kappa})}{\partial\kappa_i \partial\kappa_j}(s_k(\boldsymbol{\kappa}) - d_k) + \frac{\partial s_k(\boldsymbol{\kappa})}{\partial\kappa_i}\frac{\partial s_k(\boldsymbol{\kappa})}{\partial\kappa_j}\right)\right]. \tag{17}$$

$\mathrm{d}f(\boldsymbol{\kappa})/\mathrm{d}\boldsymbol{\kappa}$ is sometimes called sensitivity, which has to vanish in the local minimum $\boldsymbol{\kappa}^*$, see Eq. (9). The confidence interval is determined by

$$\boldsymbol{\kappa}_{\mathrm{conf}} = \boldsymbol{\kappa}^* \pm \Delta\boldsymbol{\kappa} \tag{18}$$

with

$$\Delta\kappa_i = \sqrt{P_{ii}}, \quad i = 1, \ldots, n_{\mathrm{d}}, \tag{19}$$

and the correlation matrix by

$$\boldsymbol{C} = \left[c_{ij}\right] \quad \text{with} \quad c_{ij} = \frac{P_{ij}}{\sqrt{P_{ii}}\sqrt{P_{jj}}}, \quad i, j = 1, \ldots, n_\kappa. \tag{20}$$

The diagonal terms are $c_{ii} = 1$, and the off-diagonal elements represent the linear correlation between the parameters κ_i and κ_j, $|c_{ij}| \leq 1$. The correlation matrix only makes sense if the Hessian is regular and the standard deviation is nonzero.

The property of identifiability is discussed in [5], connected to the question of the existence of a unique local minimum, see [7] for detailed investigations as well. In the following, we assume that the constraints (2) are not active. It is shown that to fulfill the necessary condition (9) and for non-vanishing and positive definite sub-determinants of the Hessian,

$$D_r = \begin{vmatrix} H_{11} & H_{12} & \ldots & H_{1r} \\ H_{21} & H_{22} & \ldots & H_{2r} \\ \vdots & & & \vdots \\ H_{r1} & H_{r2} & \ldots & H_{rr} \end{vmatrix}, \tag{21}$$

i.e., $D_r > 0$ for $r = 1, \ldots, n_\kappa$, a unique local minimum exists. For $\det \boldsymbol{H}(\boldsymbol{\kappa}^*) = 0$, there might exist a minimum, but it is not unique (as shown in the examples later on). One difficulty in real situations is to decide whether the determinant is exactly zero or whether the problem is very ill-conditioned. Since we are looking for analytical solutions, no particular discussion is followed in the subsequent investigations. Alternatively to the Hessian in Eq. (17), the Hessian can be approximated by

$$\boldsymbol{H} \approx \boldsymbol{J}^T \boldsymbol{J} = \left[\frac{\partial s_k(\boldsymbol{\kappa})}{\partial \kappa_i} \frac{\partial s_k(\boldsymbol{\kappa})}{\partial \kappa_j}\right] \tag{22}$$

for small terms $\partial^2 s_k / \partial\kappa_i \partial\kappa_j (s_k - d_k)$ (in comparison to $\boldsymbol{J}^T\boldsymbol{J}$), or in linear least-square problems by $\boldsymbol{H} = \boldsymbol{A}^T\boldsymbol{A}$.

In a few examples, the sensitivities $\boldsymbol{J}$ can be provided analytically. However, the expenditure can be very large for more complex problems—such as in finite element computations to solve initial boundary value problems—where $\boldsymbol{s}$ is implicitly defined. In this case, a common approach is to rely on numerical differentiation to obtain the Jacobian,

$$J_{ij} = \frac{\partial s_i}{\partial \kappa_j} \approx \frac{s_i(\boldsymbol{\kappa} + \Delta\kappa_j \boldsymbol{e}_j) - s_i(\boldsymbol{\kappa})}{\Delta\kappa_j}, \tag{23}$$

where $\Delta\kappa_j$ depends on the precision of the chosen programs, see [20,59]. $\boldsymbol{e}_j \in \mathbb{R}^{n_\kappa}$ contains zeros; only at the entry j there is a one. The vector $\boldsymbol{s}$ can contain reaction forces and/or displacements (or even strains).

3 Basic problems in small-strain elasticity

The aforementioned identification is studied at problems of linear, isotropic elasticity. In this case, we have the stress–strain relation

$$\mathbf{T} = K(\operatorname{tr}\mathbf{E})\mathbf{I} + 2G\mathbf{E}^D = \frac{E}{1+\nu}\left(\mathbf{E} + \frac{\nu}{1-2\nu}(\operatorname{tr}\mathbf{E})\mathbf{I}\right), \tag{24}$$

where $K = E/(3(1-2\nu))$ represents the bulk modulus and $G = E/(2(1+\nu))$ defines the shear modulus (E is the Young (elastic) modulus and ν the Poisson's ratio). The representation $(24)_1$ of the elasticity relation is common in numerical treatment, e.g., in models of viscoplasticity or viscoelasticity. $\operatorname{tr}\mathbf{E} = \varepsilon_{11} + \varepsilon_{22} + \varepsilon_{33}$ represents the trace operator of the linearized strain tensor $\mathbf{E} = (\operatorname{grad}\mathbf{u}(\mathbf{x}) + \operatorname{grad}^T\mathbf{u}(\mathbf{x}))/2$, physically defining the volumetric strain. $\mathbf{E}^D = \mathbf{E} - \big((\operatorname{tr}\mathbf{E})/3\big)\mathbf{I}$ is the deviator operator.

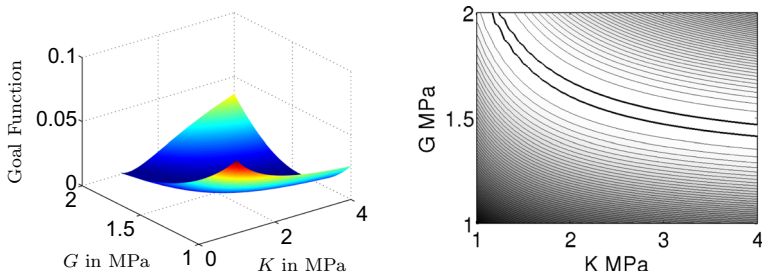

(a) **(b)**

Fig. 1 Pure axial experimental information in tensile test. **a** Surface plot $f(K, G)$, **b** contour plot $f(K, G)$

In the following, we discuss the properties of how the material parameters K and G (or E and ν) can be identified in simple tension, two-layered specimens under tensile load, torsion, and thick-walled tubes under internal pressure (with one or two layers). To investigate identifiability, we generate model data with the known parameters K and G and try to re-identify them ($K = 3$ MPa, $G = 1.5$ MPa, i.e., $E = 3.8571$ MPa and $\nu = 0.2857$).

3.1 Uniaxial tensile test

If we assume a uniaxial tensile problem in x_1-direction (compression is concluded as well), we obtain from Eq. (24)

$$\sigma_{11} = E\varepsilon_{11} = \frac{9KG}{3K+G}\varepsilon_{11}, \qquad \varepsilon_{22} = \varepsilon_{33} = -\nu\varepsilon_{11} = -\frac{3K-2G}{6K+2G}\varepsilon_{11}, \tag{25}$$

i.e., $\sigma_{11} = h(\varepsilon_{11}, K, G)$ and $\varepsilon_{22} = g(\varepsilon_{11}, K, G)$. This equation is investigated with regard to the covariance matrix and identifiability. In the first example, we consider only the (experimental) information in axial direction, and, in the second example, we have both axial and lateral experimental information.

3.1.1 Pure axial information

Let us assume that we have only two points, i.e., the given strains $\varepsilon/2$ and ε, at which the experimental data are provided, $(\varepsilon/2, d_1)$ and (ε, d_2). d_1 and d_2 are the experimental measurements, i.e., the stresses at the strain levels $\varepsilon/2$ and ε. We assume exact stress data, i.e., the first term in the Hessian (17) vanishes. The Jacobian reads

$$\boldsymbol{J}(\boldsymbol{\kappa}) = \begin{bmatrix} \dfrac{\partial h(\varepsilon/2, K, G)}{\partial K} & \dfrac{\partial h(\varepsilon/2, K, G)}{\partial G} \\ \dfrac{\partial h(\varepsilon, K, G)}{\partial K} & \dfrac{\partial h(\varepsilon, K, G)}{\partial G} \end{bmatrix} = \begin{bmatrix} \dfrac{9G^2\varepsilon}{2\,(G+3\,K)^2} & \dfrac{27K^2\varepsilon}{2\,(G+3\,K)^2} \\ \dfrac{9G^2\varepsilon}{(G+3\,K)^2} & \dfrac{27K^2\varepsilon}{(G+3\,K)^2} \end{bmatrix}, \tag{26}$$

i.e., the Hessian reads

$$\boldsymbol{H} = \boldsymbol{J}^T\boldsymbol{J} = \begin{bmatrix} \dfrac{405G^4\varepsilon^2}{4(G+3K)^4} & \dfrac{1215G^2K^2\varepsilon^2}{4(G+3K)^4} \\ \text{sym.} & \dfrac{3645K^4\varepsilon^2}{4(G+3K)^4} \end{bmatrix} \tag{27}$$

having the determinant $\det \boldsymbol{H} = 0$. This means that there is no unique local minimum. Figure 1 shows this property by plotting the goal function $f(K, G), \boldsymbol{\kappa}^T = \{K, G\}$. Here, the "valley," see contour plot 1b, demonstrates that there is no local solution and that there is an infinite number of possible K and G combinations. The missing information of the lateral strain does not lead to a local minimum. Of course, if we take the model expressed with the Young modulus and the Poisson ratio, which represents a linear least-square problem in this case, the missing information of the lateral strains would immediately indicate that ν is indeterminable. However, this very simple problem emphasizes that an identifiability study has to be performed for nonlinear identification problems and more complex boundary value problems.

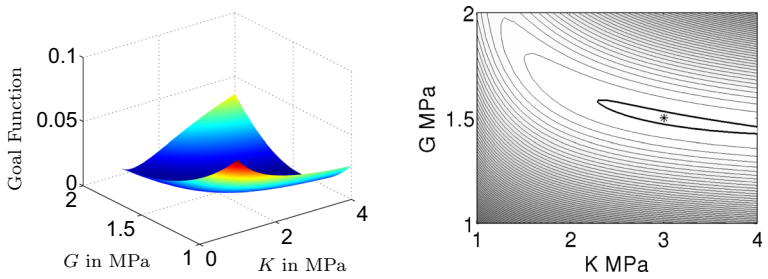

(a) **(b)**

Fig. 2 Axial and lateral information in tensile test. **a** Surface plot $f(K, G)$, **b** contour plot $f(K, G)$

3.1.2 Axial and lateral information

In the following, we provide, apart from the axial information, the lateral contraction as additional data for the identification problem. The lateral strain is given in Eq. $(25)_2$. We prescribe exact data at $\varepsilon/2$ and ε. This leads to the Jacobian

$$\boldsymbol{J}(\boldsymbol{\kappa}) = \begin{bmatrix} \dfrac{\partial h(\varepsilon/2, K, G)}{\partial K} & \dfrac{\partial h(\varepsilon/2, K, G)}{\partial G} \\ \dfrac{\partial h(\varepsilon, K, G)}{\partial K} & \dfrac{\partial h(\varepsilon, K, G)}{\partial G} \\ \dfrac{\partial g(\varepsilon/2, K, G)}{\partial K} & \dfrac{\partial g(\varepsilon/2, K, G)}{\partial G} \\ \dfrac{\partial g(\varepsilon, K, G)}{\partial K} & \dfrac{\partial g(\varepsilon, K, G)}{\partial G} \end{bmatrix} = \begin{bmatrix} \dfrac{9G^2\varepsilon}{2(G+3K)^2} & \dfrac{27K^2\varepsilon}{2(G+3K)^2} \\ \dfrac{9G^2\varepsilon}{(G+3K)^2} & \dfrac{27K^2\varepsilon}{(G+3K)^2} \\ -\dfrac{9G\varepsilon}{4(G+3K)^2} & \dfrac{9K\varepsilon}{4(G+3K)^2} \\ -\dfrac{9G\varepsilon}{2(G+3K)^2} & \dfrac{9K\varepsilon}{2(G+3K)^2} \end{bmatrix} \tag{28}$$

and the Hessian

$$\boldsymbol{H} = \boldsymbol{J}^T\boldsymbol{J} = \begin{bmatrix} \dfrac{405G^2\varepsilon^2\left(4G^2+1\right)}{16(G+3K)^4} & \dfrac{405GK\varepsilon^2\left(12GK-1\right)}{16(G+3K)^4} \\ \text{sym.} & \dfrac{405K^2\varepsilon^2\left(36K^2+1\right)}{16(G+3K)^4} \end{bmatrix}. \tag{29}$$

Here, it should be noted that the different dimensions are the result of mixing length and stress residuals, which can be circumvented by inserting a diagonal weighting matrix. Such kind of diagonal weighting matrix has no influence on the notion of identifiability, see [5]. Thus, we ignore this in our investigations. Now, the determinant of the Hessian (29) reads

$$\det \boldsymbol{H} = \frac{164025G^2K^2\varepsilon^4}{64(G+3K)^6}, \tag{30}$$

and none of the sub-determinant vanish (and they are all positive). Figure 2 shows that there is only one minimum and that re-identification is successful.

3.1.3 Axial and lateral information with perturbed data

Commonly, experimental data are not exact. We perturb the data of the example in Sect. 3.1.2 by a standard deviation of 3%, see Fig. 3a, b

in axial and lateral direction, and perform a re-identification. In this case, we obtain a very good identification, $R^2 = 0.999$, with the material parameters $K = 2.956 \pm 0.18$ MPa and $G = 1.501 \pm 0.016$ MPa instead of $K = 3$ MPa and $G = 1.5$ MPa . The determinant of the approximated Hessian (22) is $\det \boldsymbol{H} \approx 1.1 \times 10^{-8}$ and the variance $\sigma^2 = 1.18 \times 10^{-7}$. The correlation between the parameter is very small, see Eq. (20),

$$\boldsymbol{C} = \begin{bmatrix} 1 & -0.9294 \\ -0.9294 & 1 \end{bmatrix}.$$

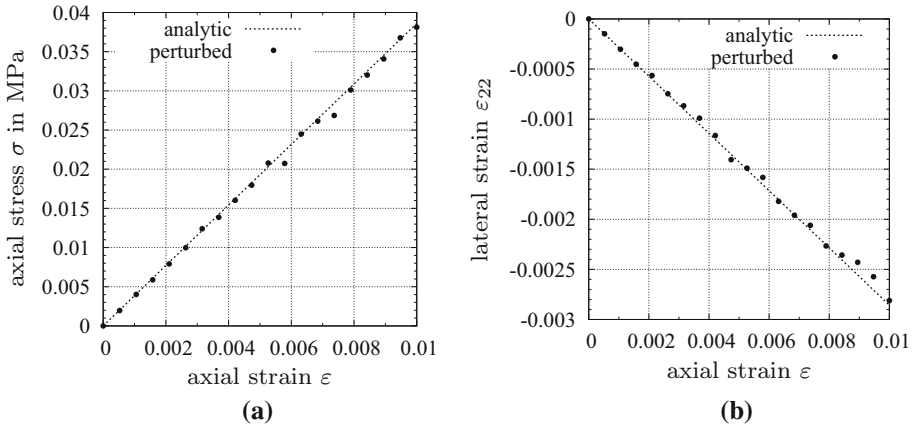

Fig. 3 Perturbed axial and lateral data in tensile test. **a** Axial stress–strain diagram, **b** lateral strain/axial strain diagram

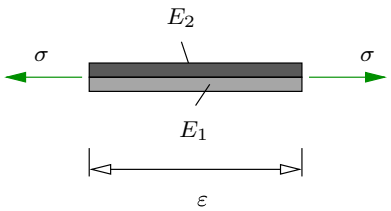

Fig. 4 Two materials in parallel

This indicates that the material parameters K and G correlate on the basis of the given experimental data. If we would determine the parameter set (E, ν) for these data, the correlation matrix is an identity matrix, i.e., there is no correlation between those parameters, which are directly addressed by the experimental data.

3.1.4 Two-layered materials

In the case of two-layered materials, for instance in bi-metallic strips, layered functionally graded polymers or even biomechanical applications such as arteries, there are layers with different material properties. The question that has to be discussed is how to determine the material parameters if only specimens with layered materials can be provided. We bear in mind the identification of the material parameters in arteries (which has been an unsolved problem so far), but the following investigations are more general and directly extendable to other materials. First, we consider a tensile test of a two-layered material, see Fig. 4. With regard to arteries, this can be interpreted as the *ring test*, see [16–18].

We again assume two prescribed strains $\varepsilon/2$ and ε. Let E_1 and E_2 be the Young moduli of the two materials that are in parallel. The total stress is the sum of two contributions,

$$\sigma = \sigma_1 + \sigma_2 = E_1\varepsilon + E_2\varepsilon = h(\varepsilon, E_1, E_2) = (E_1 + E_2)\varepsilon. \tag{31}$$

The Jacobian reads

$$\boldsymbol{J} = \begin{bmatrix} \dfrac{\partial h(\varepsilon/2, E_1, E_2)}{\partial E_1} & \dfrac{\partial h(\varepsilon/2, E_1, E_2)}{\partial E_2} \\ \dfrac{\partial h(\varepsilon, E_1, E_2)}{\partial E_1} & \dfrac{\partial h(\varepsilon, E_1, E_2)}{\partial E_2} \end{bmatrix} = \begin{bmatrix} E_2(\varepsilon/2) & E_1(\varepsilon/2) \\ E_2\varepsilon & E_1\varepsilon \end{bmatrix} \tag{32}$$

and the Hessian (for $\boldsymbol{s} - \boldsymbol{d} = \boldsymbol{0}$, i.e., exact experimental data points) is given by

$$\boldsymbol{H} = \boldsymbol{J}^T\boldsymbol{J} = \begin{bmatrix} E_2^2 & E_1E_2 \\ E_1E_2 & E_1^2 \end{bmatrix} \frac{5\varepsilon^2}{4} \tag{33}$$

i.e., $\det \boldsymbol{H} = 0$ once again indicates that there is no unique solution. This property also transfers to the constitutive equations modeled with $\boldsymbol{\kappa}^T = \{K_1, G_1, K_2, G_2\}$. Thus, we cannot expect unique material parameters

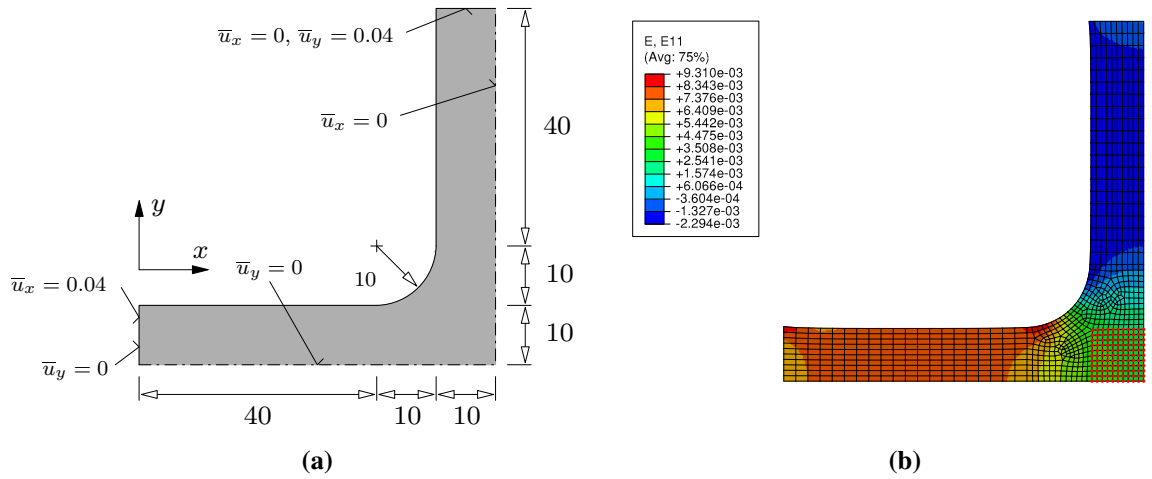

Fig. 5 Biaxial tensile test. **a** Geometry and boundary conditions (measures in mm), **b** strains ε_{xx}

for a layered material from a tensile test since we have only a globally (integral) measured force and no measured stresses within each layer. This property is also transferred to identification processes using entire finite element simulations on the basis of large strain models (compressible Neo-Hookean) using only the force–displacement data.

3.2 Torsion and bending

The case of torsion of circular tubes leads to a linear distribution of the shear stress over the radius in the case of linear elasticity. The usage of thin-walled tubes justifies the assumption of a constant shear stress (approximation), see, for example, [76],

$$M_T = G \frac{I_T}{L_0} \vartheta, \tag{34}$$

where M_T is the torque, ϑ the torsional angle, $I_T = 2\pi R^3 d$ the polar moment of inertia, R the mean radius, d the tube's wall thickness, and L_0 the height (or length) of the specimen. Obviously, we are only able to determine the shear modulus G, i.e., only a combined tension–torsion experiment is able to provide both the elastic modulus and the shear modulus. For a layered tube under tension and torsion, it is not possible to determine all the four material parameters if we measure only integral quantities such as the axial force and the resulting torque, see discussion in Sect. 3.1.4.

Regarding the bending of beams with small deformations, the analytical model (without considering shear deformations) can only provide the Young modulus, since the deflection depends on one material parameter. Thus, identifiability for two material parameters (E and ν or K and G) cannot be expected. This holds for a two-(or multi-)layered beam as well.

3.3 Biaxial tensile tests

Biaxial tensile experiments are a growing testing environment, which is mainly driven by digital full-field measurement systems (digital image correlation—DIC). For applications involving metal specimens, see, for instance, [27], or regarding polymer foils, for example, [43,58], and the literature cited therein. Biaxial tensile tests are not appropriate for developing new constitutive models, since there is no known stress state in the center region of the specimens. For known models, however, it is well suitable for material parameter identification purposes, see, for example, [65,66].

Figure 5a shows a quarter of a cruciform specimen, which is subsequently investigated (thickness $t = 1$ mm). In the following, we perform four re-identification process, where the finite element computations are done with $E = 3.8571$ MPa and $\nu = 0.2857$ for the forward problem (representing $K = 3$ MPa and $G = 1.5$ MPa).

3.3.1 Equibiaxial tests and re-identification using exact force data

In our first example, we apply the displacements $u_x = u_y = 0.4\,\text{mm}$ at the end of both arms—one quarter of the specimen—and measure the resulting force at the arms F_x and F_y, which are identical in the equibiaxial case identical, $F_x = F_y$. This means that we have only integral quantities. The result of re-identification is $\det \boldsymbol{H} \approx 0$, implying no local unique minimum. In other words, the material parameters E and ν are not uniquely identifiable (which holds for k and G as well). This corresponds to the analytical estimation of an equibiaxial plane stress problem. For $\sigma_{zz} = \tau_{xz} = \tau_{yz} = 0$, we obtain from Eq. (24)

$$\begin{Bmatrix} \sigma_{xx} \\ \sigma_{yy} \\ \tau_{xy} \end{Bmatrix} = \frac{E}{1-\nu^2} \begin{bmatrix} 1 & \nu & 0 \\ \nu & 1 & 0 \\ 0 & 0 & \frac{1-\nu}{2} \end{bmatrix} \begin{Bmatrix} \varepsilon_{xx} \\ \varepsilon_{yy} \\ \gamma_{xy} \end{Bmatrix}. \tag{35}$$

The symmetry assumption $\sigma := \sigma_{xx} = \sigma_{yy}$ and $\varepsilon := \varepsilon_{xx} = \varepsilon_{yy}$ as well as $\gamma_{xy} = 0$ yields

$$\sigma = \frac{E}{1-\nu}\varepsilon, \tag{36}$$

i.e., only one equation (one information) to determine two material parameters. Thus, a non-equibiaxial test has to be carried out to obtain more information.

3.3.2 Biaxial tests and re-identification using exact force data

If we perform a biaxial tensile test with $u_x = 0.4\text{mm}$ (horizontal arm) and $u_y = u_x/2$ (vertical arm), we obtain for the measured forces $F_x \neq F_y$ a non-vanishing determinant of the Hessian, $\det \boldsymbol{H} \approx 7.3 \times 10^{-6}$, and an exact representation of the "experimental" data, $R^2 = 1$. The prescribed material parameters can be re-identified exactly, and the confidence interval is zero for both parameters.

3.3.3 Biaxial tests and re-identification using perturbed force data and clamping displacements

The aforementioned investigation is extended to the case where the force data of F_x and F_y is perturbed (10 data points are chosen), and we prescribe the displacements at the arms (displacements of the clamps). In this case, the Young's modulus is computed to $E = 3.97 \pm 0.01$ and $\nu = 0.27 \pm 0.12$, i.e., the confidence interval, particularly of the Poisson ratio, indicates a strong correlation between the values (correlation coefficient $C_{12} = -0.89$, $\sigma^2 = 0.58 \times 10^{-4}$, $\det \boldsymbol{H} = 0.0001$. To choose only resulting forces does not lead to reliable material parameters.

3.3.4 Biaxial tests and re-identification using perturbed force data and surface displacements

If we also exploit the information of a DIC-system, i.e., we take the inplane surface displacements in a center region (here, we take the nodal displacements of the direct problem—the quadrilateral region of the mesh in the center), and the force data—both are perturbed by a standard deviation of 3% (10 data points)—and perform a test for $u_x = 0.4\,\text{mm}$ (horizontal arm) and $u_y = u_x/2$ (vertical arm), the determinant of the Hessian does not vanish. Furthermore, we identify $E = 3.93 \pm 0.0045$ MPa and $\nu = 0.2853 \pm 0.0013$, i.e., there is only a very small confidence interval. With $\sigma^2 = 5.4 \times 10^{-7}$, the material parameters are also uncorrelated, $C_{12} = -0.23$. In other words, we can reliably identify two material parameters by a biaxial (non-equibiaxial) tensile test.

3.3.5 Equibiaxial tests and re-identification using perturbed force data and surface displacements

The previous studies pose the question whether an equibiaxial tensile test with perturbed data and surface displacement is suitable to provide enough information. We choose $u_x = u_y = 0.4\,\text{mm}$, measure both the forces F_x and F_y as well as surface displacements. The determinant of the Hessian is $\det \boldsymbol{H} = 0.0205$ (local unique minimum), and the material parameters are confidently determined, $E = 3.78 \pm 0.0024$ MPa and $\nu = 0.2853 \pm 0.0007$. Even the correlation between the parameter is negligible, $C_{12} = -0.26$.

We would like to remark that we also used exact data as an input for the identification process leading to similar properties. These results indicate that full-field information can minimize problems in identification. However, for a two-layered specimen the same problems as in the case of uniaxial tensile tests occur. Thus, in two-layered specimen problems, the parameters cannot be determined.

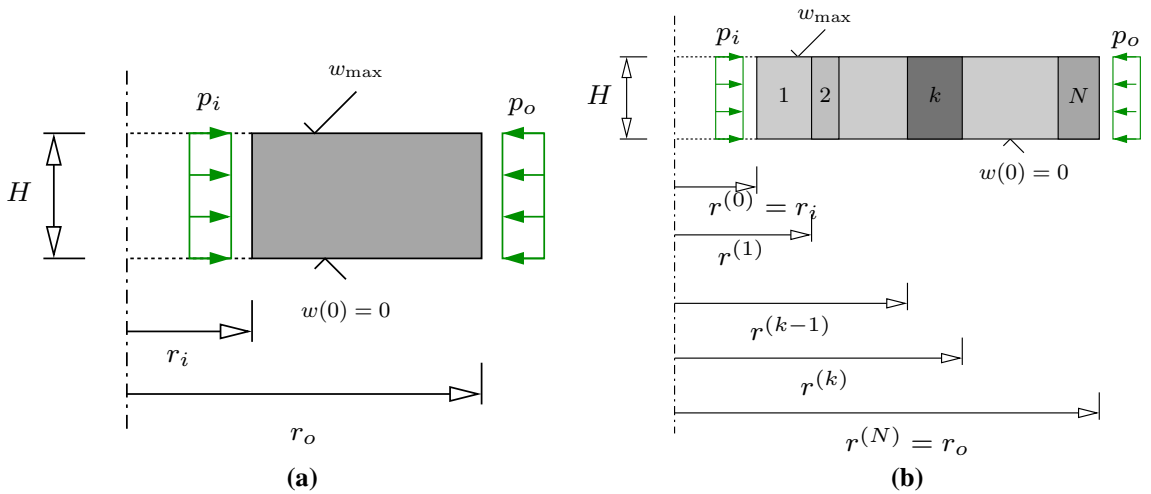

Fig. 6 Single and multi-layered thick-walled tube under internal and external pressure with axial strain

3.4 Thick-walled tube under internal pressure

A further possibility to determine the elastic material parameters might be a thick-walled tube under internal pressure p. In this case, the internal pressure is given and we can measure the radial displacements at the outer surface (either by optical measurements, see the method described in [30], or by an appropriate sensor, see [8]). Alternatively, strain gauges are applicable to determine the circumferential strains, see [12,46]. The problem of a thick-walled tube under internal pressure is an inhomogeneous deformation with the displacements at the outer surface

$$\hat{u}(r_o, p, E, \nu) = u(r_o, p, K, G) = \frac{2pr_o}{E}\frac{1-\nu^2}{d_r^2-1} = \frac{pr_o(4G+3K)}{2(d_r^2-1)(G^2+3KG)}, \tag{37}$$

and the axial stress

$$\sigma_z(p, K, G) = \frac{2p\nu}{d_r^2-1} = \frac{2p(3K-2G)}{\left(d_r^2-1\right)(2G+6K)}, \tag{38}$$

where $d_r = r_o/r_i$ is the thickness ratio of the outer and inner radius r_o and r_i, see [47] or 7 for $\varepsilon_z = 0$ and $p_o = 0$. The axial stress is constant over the radius so that the resulting force, which is measured by a testing machine, is $F_z = \sigma_z a$ with the cross section $a = \pi(r_o^2 - r_i^2)$. Figure 6a shows the boundary value problem.

3.4.1 Pure radial information

We assume that the experimental data are available for two pressures $p/2$ and p. Only the corresponding radial displacements (37) are measured at the outer radius (here, we assume $r_o = 4$ mm and $d_r = 4$). The Jacobian

$$\begin{aligned}\boldsymbol{J}(\boldsymbol{\kappa}) &= \begin{bmatrix} \dfrac{\partial u(r_o, p/2, K, G)}{\partial K} & \dfrac{\partial u(r_o, p/2, K, G)}{\partial G} \\ \dfrac{\partial u(r_o, p, K, G)}{\partial K} & \dfrac{\partial u(r_o, p, K, G)}{\partial G} \end{bmatrix} \\ &= \begin{bmatrix} -\dfrac{9pr_o}{4\left(d_r^2-1\right)(G+3K)^2} & -\dfrac{\left(4G^2+6KG+9K^2\right)pr_o}{4\left(d_r^2-1\right)G^2(G+3K)^2} \\ -\dfrac{9pr_o}{2\left(d_r^2-1\right)(G+3K)^2} & -\dfrac{\left(4G^2+6KG+9K^2\right)pr_o}{2\left(d_r^2-1\right)G^2(G+3K)^2} \end{bmatrix}\end{aligned} \tag{39}$$

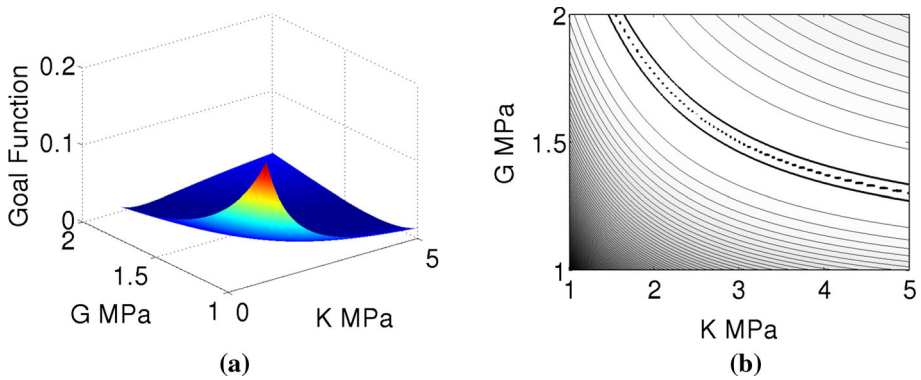

Fig. 7 Sum of squares of residuals of radial displacement (outer surface) of thick-walled tube under internal pressure, i.e., pure radial displacement information

leads to the Hessian

$$\boldsymbol{H} = \boldsymbol{J}^T \boldsymbol{J} = \begin{bmatrix} \dfrac{405 p^2 r_o^2}{16\left(d_r^2-1\right)^2 (G+3K)^4} & \dfrac{45\left(4G^2+6KG+9K^2\right) p^2 r_o^2}{16\left(d_r^2-1\right)^2 G^2 (G+3K)^4} \\ \text{sym.} & \dfrac{5\left(4G^2+6KG+9K^2\right)^2 p^2 r_o^2}{16\left(d_r^2-1\right)^2 G^4 (G+3K)^4} \end{bmatrix}. \tag{40}$$

The determinant of the Hessian vanishes $\det \boldsymbol{H} = 0$, i.e., there is no unique local minimum. In other words, additional information is necessary to obtain the material parameters K and G (similarly, this statements holds for E and ν). In Fig. 7, this property is visible in the long valley, where all material parameter combinations are valid. One possibility is, for example, an additional (separate) uniaxial tensile (or compression) test, which has to be combined with the thick-walled tube tests, or to look for a combined axially stretched and internally pressurized tube. Alternatively, a combined test can be performed, see 7.

3.4.2 Radial and axial information

In the following, the axial stresses (38) are provided in addition to the radial displacement (37). We determine the Jacobian at the internal pressure levels $p/2$ and p,

$$\begin{aligned} \boldsymbol{J}(\boldsymbol{\kappa}) &= \begin{bmatrix} \dfrac{\partial u(r_o, p/2, K, G)}{\partial K} & \dfrac{\partial u(r_o, p/2, K, G)}{\partial G} \\ \dfrac{\partial u(r_o, p, K, G)}{\partial K} & \dfrac{\partial u(r_o, p, K, G)}{\partial G} \\ \dfrac{\partial \sigma_z(p/2, K, G)}{\partial K} & \dfrac{\partial \sigma_z(p/2, K, G)}{\partial G} \\ \dfrac{\partial \sigma_z(p, K, G)}{\partial K} & \dfrac{\partial \sigma_z(p, K, G)}{\partial G} \end{bmatrix} \\ &= \begin{bmatrix} -\dfrac{9 p r_o}{4\left(d_r^2-1\right)(G+3K)^2} & -\dfrac{\left(4G^2+6KG+9K^2\right) p r_o}{4\left(d_r^2-1\right) G^2 (G+3K)^2} \\ -\dfrac{9 p r_o}{2\left(d_r^2-1\right)(G+3K)^2} & -\dfrac{\left(4G^2+6KG+9K^2\right) p r_o}{2\left(d_r^2-1\right) G^2 (G+3K)^2} \\ \dfrac{9Gp}{2\left(d_r^2-1\right)(G+3K)^2} & -\dfrac{9Kp}{2\left(d_r^2-1\right)(G+3K)^2} \\ \dfrac{9Gp}{\left(d_r^2-1\right)(G+3K)^2} & -\dfrac{9Kp}{\left(d_r^2-1\right)(G+3K)^2} \end{bmatrix}. \end{aligned} \tag{41}$$

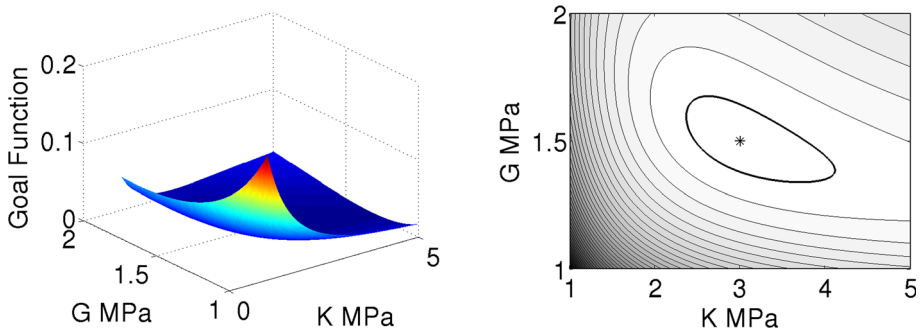

Fig. 8 Sum of squares of residuals of axial stress and radial displacement (outer surface) of thick-walled tube under internal pressure. **a** Surface plot for axial and radial information. **b** Contour plot for axial and radial information

The Hessian reads

$$\boldsymbol{H} = \begin{bmatrix} \frac{405 r_o^2 p^2}{16\left(d_r^2-1\right)^2 (G+3K)^4} + \frac{405 G^2 p^2}{4\left(d_r^2-1\right)^2 (G+3K)^4} & \frac{45\left(4G^2+6KG+9K^2\right) p^2 r_o^2}{16\left(d_r^2-1\right)^2 G^2 (G+3K)^4} - \frac{405 GK p^2}{4\left(d_r^2-1\right)^2 (G+3K)^4} \\ \text{sym.} & \frac{5\left(4G^2+6KG+9K^2\right)^2 r_o^2 p^2}{16\left(d_r^2-1\right)^2 G^4 (G+3K)^4} + \frac{405 K^2 p^2}{4\left(d_r^2-1\right)^2 (G+3K)^4} \end{bmatrix} \tag{42}$$

leading to the determinant

$$\det \boldsymbol{H} = \frac{2025 p^4 r_o^2 (4G+3K)^2}{64\left(d_r^2-1\right)^4 G^2 (G+3K)^6}. \tag{43}$$

This indicates a unique local minimum, which can be found by the optimizer, see the goal function distribution in Fig. 8.

3.4.3 Thick-walled tube with two layers

There are a number of applications of thick-walled tubes under internal and external pressure with several layers, for example in drilling applications, see [3,10,14,71,79] or in biomechanical applications such as arteries, see, for example [25,60,73]. We are interested in the question of identifiability of the material parameters in each layer. Thus, we are looking for a solution of the boundary value problem. To the best of the authors' knowledge, there is no analytical solution for the case of small-strain isotropic linear elasticity with several layers and combined axial strains. Accordingly, we provide the solution, see 8, see Fig. 6b as well.

We choose two layers, $r_i = r^{(1)} = 1$ mm, $r^{(2)} = 2$ mm and $r_o = r^{(2)} = 3$ mm, for which the internal pressure and the axial strains are provided by four (numerical experimental) points, $p_i = 1, 2, 3$ and 4 MPa, $\varepsilon_z = 1, 2, 3$ and 4%, $p_o = 0$ MPa. The resulting displacements (77) at the outer surface and the resulting axial forces (76) are computed and used for re-identification. Since we have an analytical solution, the determinant of the Hessian can be computed analytically. We omit the equations for brevity. The Mathematica result is $\det \boldsymbol{H} = 0$. Thus, there is no unique local minimum.

The main problem for small perturbed data, as an extension to the previous exact data, is that the material parameters cannot be uniquely identified again (for the latter case we have chosen $K^{(1)} = 3$ MPa, $G^{(1)} = 1.5$ MPa, $K^{(2)} = 6$ MPa, and $G^{(2)} = 3$ MPa, which are not uniquely identifiable, i.e., we obtain different results for different initial conditions).

A further investigation is to take into account the radial displacements $u(r_i)$ at the inner side ("exact" experimental data). Even in this case, $\det \boldsymbol{H} = 0$ holds. Thus, the parameters cannot be identified uniquely. This was observed for more complex constitutive models, real experimental data and a more complex geometry in the application of arteries, see [26]. There, highly correlated results are obtained, and there is also a correlation between parameters related to different layers.

3.4.4 Thick-walled tube with two layers with contour information

Following the example introduced in Sect. 3.4.3, a further investigation is performed taking into account the contour data of the outer surface of the two-layered thick-walled tube. Similar to other examples, data with and without 3% perturbation are used to re-identify the material parameters. A pressure of 1.5 MPa is applied internally, and the reaction force as well as the contour data of the outer layer is provided as the input for re-identification. The same material parameters as described in previous examples are used to create the experimental data. Axisymmetric conditions are applied. four-noded linear axisymmetric elements are used to mesh the thick-walled tube. The determinant of the Hessian is found out to be 84.99 when the exact data were used. This implies that the material parameters can be uniquely identified.

When 3% perturbed data are used to re-identify the material parameters, the determinant of the hessian is found out to be 122.12 signifying the unique identifiability of the material parameters. The material parameters are identified to be $K^{(1)} = 3.63 \pm 0.22$ MPa, $G^{(1)} = 1.5 \pm 0.06$ MPa, $K^{(2)} = 5.76 \pm 0.04$ MPa and $G^{(2)} = 2.99 \pm 0.02$ MPa. Even though the material parameters are found out to be uniquely identifiable, the identified material parameters are not as accurate when the surface information is used instead of contour information. Thus, in order to identify the material parameters with higher accuracy it is better to used surface information instead of contour information.

4 Basic problems in large strain analysis

In the following, we extend our investigations to problems, where we do not have analytical equations. Thus, we draw on finite elements to solve inhomogeneous boundary value problems similarly to Sect. 3.3. Moreover, a constitutive model for large strain theory is taken into account. The basic problems, which are identified for the small-strain experiments, transfer to the large strain case as well. Thus, we have to find a different experiment. A common testing method is to carry out indentation experiments using a hard indenter that is pressed into a weaker material to obtain the material properties (or material parameters). This is investigated for single- and two-layered specimens again.

4.1 Indentation tests: single layer

The approach of pressing an "indenter" into a material is either chosen to determine the hardness or to characterize the material behavior. For details, we refer to [13,36,37,45,61]. We are interested in the identifiability of the material parameters. Since we are talking about a problem with large strains below the indenter, we have to choose a large strain, compressible, isotropic Neo-Hookean model. The kinematics are described by the motion $\mathbf{x} = \boldsymbol{\chi}_R(\mathbf{X}, t)$, where $\mathbf{x}$ symbolizes the spatial point occupied by a material point $\mathbf{X}$ at time t. The deformation gradient $\mathbf{F}(\mathbf{X}, t) = \mathrm{Grad}\, \boldsymbol{\chi}_R(\mathbf{X}, t)$ serves as a basis to define the right Cauchy–Green tensor $\mathbf{C} = \mathbf{F}^T\mathbf{F}$. Since we are interested to have the same decomposition in the elasticity relation (volumetric strains $\varepsilon_v = \mathrm{tr}\,\mathbf{E}$ and deviatoric strains $\mathbf{E}^D$), we apply the decomposition of the deformation gradient into volume-preserving and volume-changing parts, see [23,32,57]. This implies the strain energy function

$$\psi(J, \mathrm{I}_{\overline{\mathbf{C}}}, \mathrm{II}_{\overline{\mathbf{C}}}) = U(J) + w(\mathrm{I}_{\overline{\mathbf{C}}}, \mathrm{II}_{\overline{\mathbf{C}}}) \tag{44}$$

with $J = \det \mathbf{F}$, and the invariants $\mathrm{I}_{\overline{\mathbf{C}}} = \mathrm{tr}\,\overline{\mathbf{C}}$ and $\mathrm{II}_{\overline{\mathbf{C}}} = 1/2(\mathrm{I}^2_{\overline{\mathbf{C}}} - \mathrm{tr}\,\overline{\mathbf{C}}^2)$ of the unimodular right Cauchy–Green tensor $\overline{\mathbf{C}} = (\det \mathbf{C})^{-1/3}\mathbf{C}$. Since we are using the commercial finite element program Abaqus, we choose

$$U(J) = K/2(J-1)^2 \quad \text{and} \quad w(\mathrm{I}_{\overline{\mathbf{C}}}) = \frac{G}{2}(\mathrm{I}_{\overline{\mathbf{C}}} - 3). \tag{45}$$

The resulting Cauchy stress state reads

$$\mathbf{T} = K(J-1)\mathbf{I} + \frac{G}{J}\overline{\mathbf{B}}^D \tag{46}$$

with the unimodular left Cauchy–Green tensor $\overline{\mathbf{B}} = (\det \mathbf{B})^{-1/3}\mathbf{B}$, $\mathbf{B} = \mathbf{F}\mathbf{F}^T$. In the case of small strains, the linearized constitutive model (46) leads to Eq. (24).

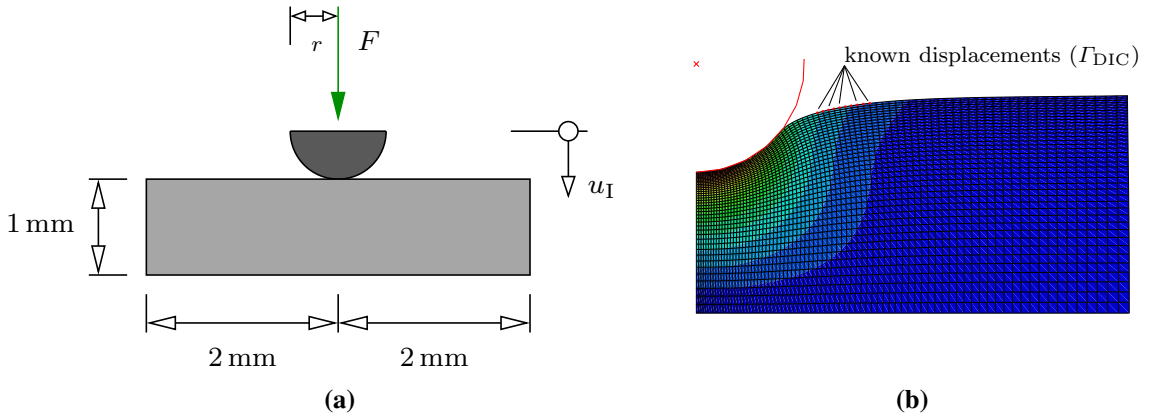

Fig. 9 Geometry and simulation result of indentation test (indenter radius $r = 0.5$ mm, indentation depth $u_\mathrm{I} = 0.35$ mm). **a** Geometry. **b** Mesh and result of finite element solution

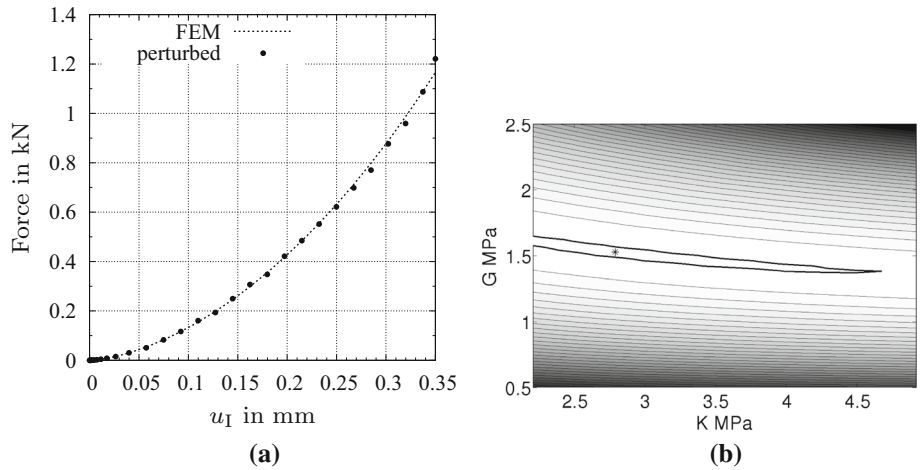

Fig. 10 Perturbed force for indentation test and contour plot of $f(K, G)$. **a** Force–displacement behavior and perturbed data. **b** Goal function behavior for indentation test with "measured perturbed" force

We have to identify the bulk modulus K and shear modulus G from a displacement-controlled process. $u_\mathrm{I} = 0.35$ mm is the indentation depth, see the sketch in Fig. 9a for the geometrical data.

The entire specimen is assumed to be axisymmetric, and the indenter is given as a rigid spherical indenter with the radius $r = 0.5$ mm. The element type used is CAX4R (4-noded bilinear quadrilateral elements) with reduced integration and a total number of 3321 nodes as shown in Fig. 9b. Surface-to-surface contact is chosen in connection with a node-to-surface contact discretization method and a tangential frictional coefficient of 0.4.

4.1.1 Pure re-identification

If we indent the ball into the material with $K = 3$ MPa and $G = 1.5$ MPa, a number of points are generated by the automatic load control of Abaqus. The force indentation depth information F/u_I is chosen to re-identify the material parameters. In this case, we obtain the material parameters with four-digit accuracy and an $R^2 = 1$ value. The determinant of the Hessian is $\det \boldsymbol{H} \approx 1.56$. Thus, it seems that we have a reliable test for identifying K and G.

4.1.2 Re-identification using perturbed force data

Now, we perturb the force data with a standard deviation of 3%, see Fig. 10a, and try to re-identify the material parameters. This leads, with the initial guess of $K^{(0)} = 7.499$ MPa and $G^{(0)} = 0.9$ MPa, to the result of identification $K = 2.12 \pm 0.21$ MPa and $G = 1.63 \pm 0.04$ MPa (instead of the expected parameters

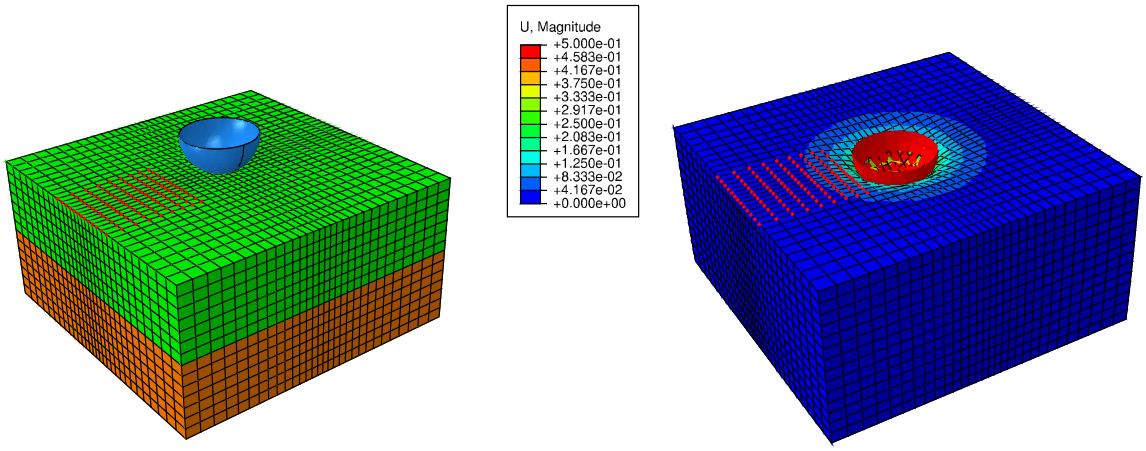

(a) **(b)**

Fig. 11 Geometry, mesh and displacement of three-dimensional two-layered plate under indentation. **a** Layer distribution and mesh, **b** maximum displacement distribution

$K = 3$ MPa and $G = 1.5$ MPa). The material parameters are also highly correlated (correlation coefficient $C_{12} = 0.995$) indicating that the identification process is highly sensitive. If we vary the input material parameters K and G to compute the goal function $f(K, G)$, we are able to see the minimum at the contour plot shown in Fig. 10b. The minimum is located in a very narrow, elongated valley. Since the valley is almost parallel to the K-axis, the confidence interval is also larger for K than for G, i.e., the estimation of K is more uncertain.

4.1.3 Perturbed data and surface deformation

Apart from the measured reaction force F, we assume that a digital image correlation system can measure the radial and axial displacement in a small region Γ_{DIC} close to the indenter, see Fig. 9b, to obtain a bite more information than only the force–indentation depth curve. The displacement on Γ_{DIC} and the reaction forces F are used to identify the material parameters (29 load steps). Now, the Jacobian is computed numerically using Eq. (23). The resulting Hessian and its determinant of the re-identification are

$$\boldsymbol{H} = \begin{bmatrix} 49.81 & -12.24 \\ -12.24 & 3.21 \end{bmatrix}, \quad \text{and} \quad \det \boldsymbol{H} = 9.856 \tag{47}$$

indicating that identifiability is guaranteed at this point. However, with a variance of $\sigma^2 = 6.12 \times 10^{-5}$, all data are perturbed with a standard deviation of 3%, and the correlation between the material parameters is again extremely high,

$$\boldsymbol{C} = \begin{bmatrix} 1 & 0.9687 \\ 0.9687 & 1 \end{bmatrix}. \tag{48}$$

Thus, the incorporation of further information does, in this example, only slightly improve the confidence interval, $G = 1.52 \pm 4.5 \times 10^{-3}$ MPa, $K = 2.79 \pm 1.8 \times 10^{-2}$ MPa, but not the correlation between the parameters.

4.2 Two-layer application

The results of the identification of the single-layer discussion in Sect. 4.1 allow us to be optimistic about obtaining elastic material parameters for a two-layered material. Here, we assume that the material is soft so that surface deformations are large enough to be detectable by a digital image correlation system. Figure 11a shows the three-dimensional discretization, which yields much more information than the axisymmetric consideration of Sect. 4.1, where the block is 4 mm $\times$ 4 mm with a height of 2 $\times$ 1 mm. A typical displacement is shown in Fig. 11b. The element type used is C3D8 (8-noded brick elements). Let us carry out two tests: first,

the displacement-controlled indentation is performed at layer 1 and, afterward, at layer 2 ($u_{\mathrm{I}} = 0.5$mm). Furthermore, we choose a larger indentation than in Sect. 4.1 to initiate larger deformations at the surface. Again, the force data and surface displacements are generated, perturbed and afterward provided for re-identification. Here, we have the material parameters $K^{(1)} = 3$ MPa, $G^{(1)} = 1.5$ MPa, $K^{(2)} = 6$ MPa and $G^{(2)} = 3$ MPa. The result of identification is $K^{(1)}_{\mathrm{res}} = 2.91 \pm 0.05$ MPa, $G^{(1)}_{\mathrm{res}} = 1.52 \pm 0.0076$ MPa, $K^{(2)}_{\mathrm{res}} = 5.98 \pm 0.1$ MPa, and $G^{(2)}_{\mathrm{res}} = 3.04 \pm 0.0097$ MPa. Additionally, we have a very good fit $R^2 = 0.999$, a non-vanishing determinant of the Hessian, $\det \boldsymbol{H} = 0.803$, and a correlation matrix ($\sigma^2 = 0.0001$)

$$\boldsymbol{C} = \begin{bmatrix} 1 & 0.64 & -0.23 & -0.21 \\ & 1 & -0.05 & -0.59 \\ & & 1 & 0.25 \\ & & & 1 \end{bmatrix}.$$

The correlation is moderate, so that this test seems to be suitable to reliably identify the elastic material parameters of a Neo-Hookean-type model with weak stiffness and DIC-data on the surface. However, for more complex material models (plasticity, …, anisotropy) this statement cannot be generalized since the number of material parameters is higher and additional investigations are required.

5 Conclusions

Nowadays, it is common to apply optimization routines to various experimental test data in order to identify the material parameters of complex constitutive models. If the test data show inhomogeneous deformation, finite elements are chosen to solve the boundary value problem. Commonly, these routines provide material parameters. A first simple approach to obtain indications about the quality of the identification is the R^2-value, which provides information about how well the model represents the experimental data. However, this information is not enough, since we have to discuss both whether the problem leads to (local) identifiability and to the correlation of the material parameters as well as the confidence interval. In this paper, we investigate this in the scope of classical tests with specimens of one and two layers of different elastic materials (uniaxial tension or compression, shear, torsion, bending, biaxial tensile tests, tubes under internal pressure and the indentation of a ball indenter). We restrict ourselves to the most simplest constitutive model of linear, isotropic elasticity (Hooke's law) for small strains and a compressible Neo-Hookean-type hyperelasticity model at finite strains, which both only have two material parameters.

It turns out that, in order to identify both material parameters (small-strain, linear isotropic elasticity) of a single-layered specimen, we have to perform a uniaxial tensile test either in combination with lateral strain measurement, with torsion or with a shear experiment. The combination depends essentially on the available specimens and testing devices. If biaxial tensile tests are performed, we require the surface deformation. Pure displacement information of the testing machine's traverse leads, with regard to parameter identification, only to success for a non-equibiaxial tensile test. An experiment of a tube under internal pressure also requires, apart from the radial displacement outside, the axial force information.

It is very difficult—sometimes even impossible—to identify the material parameters of each material in a two-layered specimen using classical tests. Only if we have a soft material, where a two-sided ball indentation test is able to initiate large deformations on the surface, we might obtain the parameters that are weakly correlated.

All these statements hold for very simple constitutive models. If we have models of internal variable type with evolution equations describing the hardening behavior, this becomes much more difficult. Thus, the indicators of the R^2, the determinant of the Hessian (up to a certain sense) and the correlation coefficients can provide helpful insights. For example, in [62] these indicators are chosen also for neglecting terms in constitutive equations during the phase of modeling if the experiments cannot provide more information. Moreover, experiments have to be separated into sub-problems (modes), and a subset of parameters has to be identified in each of these sub-problems. Thus, material parameter identification is a complicated process that requires expert knowledge regarding the possible experiments, the properties of the optimization tools, the interpretation of optimization indicators and the model behavior.

Acknowledgements We would like to express out sincere thanks to the German–Israeli Foundation for Scientific Research and Development (GIF) for their financial support of the project.

Appendix

7 Thick-walled tube under internal and external pressure and axial strains

The analytical solution of the thick-walled tube under both agencies, internal and external pressure and axial strains for isotropic, linear elasticity in the small-strain regime, is recapped, since it is required for the more general multi-layered results in 8, see references cited in [80] as well. We assume a displacement field

$$\mathbf{u}(r, z) = u(r)\mathbf{e}_r + w(z)\mathbf{e}_z, \tag{49}$$

leading to the linearized Green strain tensor $\mathbf{E} = u_{,r}\,\mathbf{e}_r \otimes \mathbf{e}_r + (u/r)\mathbf{e}_\vartheta \otimes \mathbf{e}_\vartheta + w_{,z}\,\mathbf{e}_z \otimes \mathbf{e}_z$. r, ϑ, z are cylindrical coordinates, $\mathbf{e}_r$, $\mathbf{e}_\vartheta$ and $\mathbf{e}_z$ the normalized tangent vectors in radial, circumferential and axial direction. The notation $u_{,r}$ symbolizes the partial derivative of the radial displacement u with respect to r, $u_{,r} = \partial u/\partial r$. $u(r)$ is unknown and $w(0) = 0$ and $w(H) = w_{\max}$ are prescribed (H is the thickness of the circular plate), see Fig. 6a. The radial and circumferential strains are $\varepsilon_r = u_{,r}$ and $\varepsilon_\vartheta = u/r$, respectively, and the axial strain $\varepsilon_z = w_{,z} = \text{const.}$ is assumed to be constant over z. Using the elasticity relation (24), we have

$$\begin{aligned}
\sigma_r &= \frac{E}{(1+\nu)(1-2\nu)}\big((1-\nu)\varepsilon_r + \nu\varepsilon_\vartheta + \nu\varepsilon_z\big),\\
\sigma_\vartheta &= \frac{E}{(1+\nu)(1-2\nu)}\big(\nu\varepsilon_r + (1-\nu)\varepsilon_\vartheta + \nu\varepsilon_z\big),\\
\sigma_z &= \frac{E}{(1+\nu)(1-2\nu)}\big(\nu\varepsilon_r + \nu\varepsilon_\vartheta + (1-\nu)\varepsilon_z\big),
\end{aligned} \tag{50}$$

or the inverse relation

$$\begin{aligned}
\varepsilon_r = u_{,r} &= \frac{1}{E}\big(\sigma_r - \nu\sigma_\vartheta - \nu\sigma_z\big),\\
\varepsilon_\vartheta = \frac{u}{r} &= \frac{1}{E}\big(-\nu\sigma_r + \sigma_\vartheta - \nu\sigma_z\big),\\
\varepsilon_z = w_{,z} &= \frac{1}{E}\big(-\nu\sigma_r - \nu\sigma_\vartheta + \sigma_z\big).
\end{aligned} \tag{51}$$

Additionally, we have to fulfill the equilibrium conditions $\operatorname{div}\mathbf{T} = \mathbf{0}$ in the absence of specific body forces, leading to

$$\begin{aligned}
\sigma_{r,r} + \frac{\sigma_r - \sigma_\vartheta}{r} = 0 \quad &\rightarrow \quad (r\sigma_r)_{,r} - \sigma_\vartheta = 0\\
\sigma_{\vartheta,\vartheta} = 0 \quad &\rightarrow \quad \sigma_\vartheta \text{ is constant over } \vartheta\\
\sigma_{z,z} = 0 \quad &\rightarrow \quad \sigma_z \text{ is constant over } z
\end{aligned} \tag{52}$$

see, for example, [54].
We insert Eqs. $(50)_1$ and $(50)_2$ into Eq. $(51)_3$ and obtain

$$\sigma_z = E\varepsilon_z + \nu(\sigma_r + \sigma_\vartheta) \tag{53}$$

leading to

$$\sigma_{z,r} = \nu(\sigma_{r,r} + \sigma_{\vartheta,r}), \tag{54}$$

because of a constant axial strain ε_z. Now, we multiply Eq. $(51)_2$ with the Young modulus E and the radial coordinate r—evaluating $\varepsilon_\vartheta = u/r$—leading to

$$Eu = r(\sigma_\vartheta - \nu\sigma_r - \nu\sigma_z). \tag{55}$$

The derivative with respect to the radial coordinate employing $u_{,r} = \varepsilon_r$ and Eq. $(51)_1$ leads to

$$Eu_{,r} = \sigma_\vartheta - \nu\sigma_r - \nu\sigma_z + r\big(\sigma_{\vartheta,r} - \nu\sigma_{r,r} - \nu\sigma_{z,r}\big) = E\varepsilon_r = \sigma_r - \nu\sigma_\vartheta - \nu\sigma_z.$$

After inserting Eq. (54), we arrive at

$$\sigma_\vartheta - \sigma_r + r(1-\nu)\sigma_{\vartheta,r} - r\nu\sigma_{r,r} = 0, \tag{56}$$

where, additionally, the equilibrium conditions $(52)_1$ have to be considered. This leads to

$$\sigma_{r},_{r} + \sigma_{\vartheta},_{r} = 0, \tag{57}$$

i.e., in view of Eq. (54), the axial stresses are constant over r, $\sigma_{z},_{r} = 0$. If we integrate Eq.(57)

$$\sigma_r + \sigma_\vartheta = 2C_1, \tag{58}$$

and again insert the circumferential stress from Eq. $(52)_1$ and multiply the relation with r, we arrive at

$$\left(r^2\sigma_r\right),_r = 2C_1 r,$$

or, if we integrate this relation, the radial stress

$$r^2\sigma_r = C_1 r^2 + C_2 \quad \Rightarrow \quad \sigma_r = C_1 + \frac{C_2}{r^2} \tag{59}$$

can be derived. Since $\sigma_{z},_{r} = 0$ vanishes, we obtain the circumferential stress from Eq. (58),

$$\sigma_\vartheta = C_1 - \frac{C_2}{r^2}. \tag{60}$$

The constants are determined by the boundary conditions

$$\begin{aligned} \sigma_r(r_i) &= -p_i = C_1 + \frac{C_2}{r_i^2} \\ \sigma_r(r_o) &= -p_o = C_1 + \frac{C_2}{r_o^2} \end{aligned} \tag{61}$$

leading to the coefficients

$$C_1 = \frac{p_i r_i^2 - p_o r_o^2}{r_o^2 - r_i^2}, \qquad C_2 = \frac{r_i^2 r_o^2}{r_o^2 - r_i^2}(p_o - p_i). \tag{62}$$

p_i and p_o are the internal and external pressure, respectively. r_i and r_o are the internal and external radius. In view of experimental results, we can measure the axial force by integrating the axial stresses (53) using Eqs. (59) and (60),

$$F_z = 2\pi \int_{r_i}^{r_o} \sigma_z(r) r \mathrm{d}r = \sigma_z a, \quad \text{with} \quad \sigma_z = E\varepsilon_z + 2\nu C_1, \tag{63}$$

with the cross section $a = \pi(r_o^2 - r_i^2)$. Additionally, the radial displacements (or the circumferential strains) on the outside are measurable,

$$u(r_o) = \frac{2r_o r_i^2(1-\nu^2)}{E(r_o^2 - r_i^2)} p_i - \frac{r_o\left(r_i^2(1+\nu) + r_o^2(1-\nu+2\nu^2)\right)}{E(r_o^2 - r_i^2)} p_o - \nu r_o \varepsilon_z. \tag{64}$$

8 Analytical solution of thick-walled cylinder with several layers

Multi-layered thick-walled tubes occur, for example, in drilling pipes, pressure vessels, or arteries. In the following, each layer k, $k = 1, \ldots, N$, is assumed to be of an isotropic, linear elastic material behavior. The layers are defined by the radius $r^{(k)}$, $k = 0, \ldots, N$, with the internal and external radius $r^{(0)} = r_i$ and $r^{(N)} = r_o$, respectively, see Fig. 6b. As in 7, we assume that the lower cut of the tube is fixed in axial direction and the upper part is stretched by $w_{\max}$. The pressures p_i and p_o are applied internally and externally. Thus, we have the boundary conditions

$$\sigma_r^{(1)}(r_i) = \sigma_r^{(1)}(r^{(0)}) = -p_i, \quad \sigma_r^{(N)}(r_o) = \sigma_r^{(1)}(r^{(N)}) = -p_0. \tag{65}$$

Additionally, the internal constraints in between the layers are given,

$$\begin{aligned} u^{(k-1)}(r^{(k-1)}) &= u^{(k)}(r^{(k-1)}), \\ \sigma_r^{(k-1)}(r^{(k-1)}) &= \sigma_r^{(k)}(r^{(k-1)}), \end{aligned} \tag{66}$$

for $k = 2, \ldots, N$. The right superscript (k), $k = 1, \ldots, N$, in the stress and displacement field, defines the layer number. In view of Eq. (59), and for the radial displacements (55) the two unknowns $C_1^{(k)}$ and $C_2^{(k)}$ have to be specified in each layer, i.e., we have a total of $2N$ unknowns. On the other hand, we have with Eqs. (65) and (66) $n_{\text{eq}} = 2(N-1) + 2 = 2N$ equations. From the conditions (65), the two equations

$$\sigma_r^{(1)}(r^{(0)}) = C_1^{(1)} + \frac{C_2^{(1)}}{r^{(0)^2}} = -p_i \tag{67}$$

$$\sigma_r^{(N)}(r^{(N)}) = C_1^{(N)} + \frac{C_2^{(N)}}{r^{(N)^2}} = -p_o \tag{68}$$

are obtained. Applying Eq. (59) for the internal constraint $(66)_2$, we arrive at

$$C_1^{(k-1)} + \frac{C_2^{(k-1)}}{r^{(k-1)^2}} = C_1^{(k)} + \frac{C_2^{(k)}}{r^{(k-1)^2}} \tag{69}$$

Next, we insert the radial, circumferential and axial stresses (59), (60) and (63) depending on the constants C_1 and C_2 into the radial displacements (55). This leads to

$$u = \frac{r}{E}\left((1 - \nu - 2\nu^2)C_1 - \frac{1+\nu}{r^2}C_2\right) - \nu r\varepsilon_z. \tag{70}$$

For each layer, the constraint $(66)_1$ yields

$$A_1^{(k-1)}C_1^{(k-1)} - \frac{A_2^{(k-1)}}{r^{(k-1)^2}}C_2^{(k-1)} - \left(A_1^{(k)}C_1^{(k)} - \frac{A_2^{(k)}}{r^{(k-1)^2}}C_2^{(k)}\right) = \left(\nu^{(k-1)} - \nu^{(k)}\right)\varepsilon_z, \tag{71}$$

with

$$A_1^{(k)} = \frac{1 - \nu^{(k)} - 2\nu^{(k)^2}}{E^{(k)}}, \quad A_2^{(k)} = \frac{1+\nu^{(k)}}{E^{(k)}}, \tag{72}$$

The combination of Eqs. (67), (68), (69) and (71) leads to the system of linear equations

$$\boldsymbol{A}\boldsymbol{c} = \boldsymbol{p}, \tag{73}$$

with

$$\boldsymbol{A} = \begin{bmatrix}
1 & \frac{1}{r^{(0)^2}} & & & & & & \\
A_1^{(1)} & -\frac{A_2^{(1)}}{r^{(1)^2}} & -A_1^{(2)} & \frac{A_2^{(2)}}{r^{(1)^2}} & & & & \\
1 & \frac{1}{r^{(1)^2}} & -1 & -\frac{1}{r^{(1)^2}} & & & & \\
 & & A_1^{(2)} & -\frac{A_2^{(2)}}{r^{(2)^2}} & -A_1^{(3)} & \frac{A_2^{(3)}}{r^{(2)^2}} & & \\
 & & 1 & \frac{1}{r^{(2)^2}} & -1 & -\frac{1}{r^{(2)^2}} & & \\
 & & & & & & \ddots & \\
 & & & & & & 1 & \frac{1}{r^{(N)^2}}
\end{bmatrix}, \tag{74}$$

and

$$\begin{aligned}
\boldsymbol{c}^T &= \left\{C_1^{(1)}, C_2^{(1)}, C_1^{(2)}, C_2^{(2)}, \ldots, C_1^{(N)}, C_2^{(N)}\right\}, \\
\boldsymbol{p}^T &= \left\{-p_i, \left(\nu^{(1)} - \nu^{(2)}\right)\varepsilon_z, 0, \left(\nu^{(2)} - \nu^{(3)}\right)\varepsilon_z, \ldots 0, -p_o\right\}.
\end{aligned} \tag{75}$$

After solving the linear system (73), we can determine the stress distribution in each layer $\sigma_r^{(k)}(r) = h_r^{(k)}(r, \boldsymbol{\kappa}, C_1^{(1)}(\boldsymbol{\kappa}), C_2^{(1)}(\boldsymbol{\kappa}), \ldots)$, $\sigma_\vartheta^{(k)}(r) = h_\vartheta^{(k)}(r, \boldsymbol{\kappa}, C_1^{(1)}(\boldsymbol{\kappa}), C_2^{(1)}(\boldsymbol{\kappa}), \ldots)$, and $\sigma_z^{(k)} = h_z^{(k)}(\boldsymbol{\kappa}, C_1^{(1)}(\boldsymbol{\kappa}), \ldots)$, and the displacements. In view of a sensitivity analysis of an experiment, the resulting force

$$F_z = 2\pi \int_{r_i}^{r_o} \sigma_z r \, \mathrm{d}r = \sum_{k=1}^{N} h_z^{(k)}(\boldsymbol{\kappa}, C_1^{(1)}(\boldsymbol{\kappa}), \ldots) a_k \tag{76}$$

with the partial cross sections of layers, $a_k = \pi\left(r^{(k)^2} - r^{(k-1)^2}\right), k = 1, \ldots, N$, can be calculated. Additionally, we can compute the outer surface displacement

$$u(r_o) = u^{(N)}(r^{(N)}) = r^{(N)}\left(A_1^{(N)} C_1^{(N)} - A_2^{(N)} C_2^{(N)}\right) - \nu^{(N)} r^{(N)} \varepsilon_z. \tag{77}$$

References

1. Amin, A.F.M.S., Alam, M.S., Okui, Y.: An improved hyperelasticity relation in modeling viscoelasticity response of natural and high damping rubbers in compression: experiments, parameter identification and numerical verification. Mech. Mater. **34**, 75–95 (2002)
2. Andresen, K., Dannemeyer, S., Friebe, H., Mahnken, R., Ritter, R., Stein, E.: Parameteridentifikation für ein plastisches Stoffgesetz mit FE-Methoden und Rasterverfahren. Bauingenieur **71**, 21–31 (1996)
3. Bai, Y., Igland, T.R., Moan, T.: Tube collapse under combined external pressure, tension and bending. Mar. Struct. **10**(5), 389–410 (1997)
4. Bazaraa, M.S., Sherali, H.D., Shetty, C.M.: Nonlinear Programming. Wiley, New York (1993)
5. Beck, J.V., Arnold, K.J.: Parameter Estimation in Engineering and Science. Wiley, New York (1977)
6. Benedix, U., Görke, U.J., Kreißig, R., Kretzschmar, S.: Local and global analysis of inhomogeneous displacement fields for the identification of material parameters. In: Hoa, S.V., De Wilde, W.P., Blain, W.R. (eds) Computer Methods in Composite Materials VI (CADCOMP 98), pp 159–168 (1998)
7. Beveridge, G.S.G., Schechter, R.S.: Optimization: Theory and Practice, 1st edn. McGraw-Hill Book Company, New York (1970)
8. Bier, W., Dariel, M.P., Frage, N., Hartmann, S., Michailov, O.: Die compaction of copper powder designed for material parameter identification. Int. J. Mech. Sci. **49**, 766–777 (2007)
9. Björck, A.: Numerical Methods for Least Squares Problems. SIAM (Society for Industrial and Applied Mathematics), Philadelphia (1996)
10. Bourgoyne, A.: Applied Drilling Engineering. Society of Petroleum Engineers, Dallas (1986). SPE textbook series
11. Calloch, S., Marquis, D.: Triaxial tension-compression tests for multiaxial cyclic plasticity. Int. J. Plast **15**, 521–549 (1999)
12. Carnavas, P.C., Page, N.W.: Elastic properties of compacted metal powders. J. Mater. Sci. **33**, 4647–4655 (1998)
13. Chen, Z., Diebels, S.: Nanoindentation of soft polymers: modeling, experiments and parameter identification. Tech. Mech. **34**, 166–189 (2014)
14. Clifton, R.J., Simonson, E.R., Jones, A.H., Green, S.J.: Determination of the critical-stress-intensity factor kic from internally pressurized thick-walled vessels. Exp. Mech. **16**(6), 233–238 (1976)
15. Coleman, B.D., Gurtin, M.E.: Thermodynamics with internal state variables. J. Chem. Phys. **47**, 597–613 (1967)
16. Consigny, P.M., Tulenko, T.N., Nicosia, R.F.: Immediate and long-term effects of angioplasty-balloon dilation on normal rabbit iliac artery. Arterioscler. Thromb. Vasc. Biol. **6**(3), 265–276 (1986)
17. Cox, R.H.: Comparison of mechanical and chemical properties of extra- and intralobar canine pulmonary arterie. Am. J. Physiol. Heart Circ. Physiol. **242**, H245–H253 (1982)
18. Cox, R.H.: Comparison of arterial wall mechanics using ring and cylindrical segments. Am. J. Physiol. Heart Circ. Physiol. **244**, H298–H303 (1983)
19. Davis, J.R.: Tensile Testing, 2nd edn. ASM International, Materials Park (2004)
20. Dennis, J.E., Schnabel, R.B.: Numerical Methods for Unconstrained Optimization and Nonlinear Equations, Classics in Applied Mathematics, vol. 16. SIAM Society for Industrial and Applied Mathematics, Philadelphia (1996)
21. Diebels, S., Chen, Z., Scheffer, T., Seibert, H.: Macroindentation of a soft polymer: identification of hyperelasticity and validation by uni/biaxial tensile tests. Mech. Mater. **64**, 111–127 (2013)
22. Draper, N.R., Smith, H.: Applied Regression Analysis, 3rd edn. Wiley, New York (1998)
23. Flory, P.J.: Thermodynamic relations for high elastic materials. Trans. Faraday Soc. **57**, 829–838 (1961)
24. Forsberg, F., Sjödahl, M., Mooser, R., Hack, E., Wyss, P.: Full three-dimensional strain measurements on wood exposed to three-point bending: analysis by use of digital volume correlation applied to synchrotron radiation micro-computed tomography image data. Strain **46**, 47–60 (2010)
25. Gasser, T.C., Ogden, R.W., Holzapfel, G.A.: Hyperelastic modelling of arterial layers with distributed collagen fibre orientations. J. R. Soc. Interface **3**(6), 15–35 (2006)
26. Gilbert, R.R., Hartmann, S., Kudela, L., Rank, E., Sahar, G., Yosibash, Z., Yossef, O.: Parameter identification of the passive response in arteries. Technical Report Series Fac3-16-01, Faculty of Mathematics/Computer Science and Mechanical Engineering, Clausthal University of Technology (Germany) (2016)
27. Hannon, A., Tiernan, P.: A review of planar biaxial tensile test systems for sheet metal. J. Mater. Process. Technol. **198**(1–3), 1–13 (2008)

28. Hartmann, S.: Numerical studies on the identification of the material parameters of Rivlin's hyperelasticity using tension–torsion tests. Acta Mech. **148**, 129–155 (2001a)
29. Hartmann, S.: Parameter estimation of hyperelasticity relations of generalized polynomial-type with constraint conditions. Int. J. Solids Struct. **38**(44–45), 7999–8018 (2001b)
30. Hartmann, S., Tschöpe, T., Schreiber, L., Haupt, P.: Large deformations of a carbon black-filled rubber. Experiment, optical measurement and parameter identification using finite elements. Eur. J. Mech. Ser. A Solids **22**, 309–324 (2003)
31. Hartmann, S., Gibmeier, J., Scholtes, B.: Experiments and material parameter identification using finite elements. Uniaxial tests and validation using instrumented indentation tests. Exp. Mech. **46**(1), 5–18 (2006)
32. Hartmann, S., Neff, P.: Polyconvexity of generalized polynomial-type hyperelastic strain energy functions for near-incompressibility. Int. J. Solids Struct. **40**(11), 2767–2791 (2003)
33. Haupt, P.: Continuum Mechanics and Theory of Materials, 2nd edn. Springer, Berlin (2002)
34. Haupt, P., Lion, A.: Experimental identification and mathematical modelling of viscoplastic material behavior. J. Contin. Mech. Thermodyn. **7**, 73–96 (1995)
35. Haupt, P., Sedlan, K.: Viscoplasticity of elastomeric materials: experimental facts and constitutive modelling. Arch. Appl. Mech. **71**, 89–109 (2001)
36. Huber, N., Tsakmakis, C.: Determination of constitutive properties from spherical indentation data using neural networks, Part I: plasticity with nonlinear and kinematic hardening. J. Mech. Phys. Solids **47**, 1589–1607 (1999a)
37. Huber, N., Tsakmakis, C.: Determination of constitutive properties from spherical indentation data using neural networks, Part II: the case of pure kinematic hardening in plasticity laws. J. Mech. Phys. Solids **47**, 1569–1588 (1999b)
38. Johlitz, M., Diebels, S., Jan, B., Steeb, H., Wulff, P.: Size effects in polyurethane bonds: experiments, modelling and parameter identification. J. Mater. Sci. **43**, 4768–4779 (2008)
39. Kadlowec, J., Wineman, A., Hulbert, G.: Elastomer bushing response: experiments and finite element modeling. Acta Mech. **163**, 25–38 (2003)
40. Krämer, S., Rothe, S., Hartmann, S.: Homogeneous stress-strain states computed by 3D-stress algorithms of FE-codes: application to material parameter identification. Eng. Comput. **31**, 141–159 (2015)
41. Kreißig, R.: Auswertung inhomogener Verschiebungsfelder zur Identifikation der Parameter elastisch-plastischer Deformationsgesetze. Forsch. Ingenieurwes. **64**, 99–109 (1998)
42. Kreissig, R., Benedix, U., Goerke, U.J.: Statistical aspects of the identification of material parameters for elasto-plastic models. Arch. Appl. Mech. **71**, 123–134 (2001)
43. Lamkanfi, E., Paepegem, W.V., Degrieck, J.: Shape optimization of a cruciform geometry for biaxial testing of polymers. Polym. Testing **41**, 7–16 (2015)
44. Lawson, C.L., Hanson, R.J.: Solving least squares problems. Siam Society for Industrial and Applied Mathematics, Philadelphia (1995)
45. Lee, H., Lee, J.H., Pharr, G.M.: A numerical approach to spherical indentation techniques for material property evaluation. J. Mech. Phys. Solids **53**, 2037–2069 (2005)
46. Lefebvre, D., Chebl, C., Thibodeau, L., Khazzari, E.: A high-strain biaxial-testing rig for thin-walled tubes under axial load and pressure. Exp. Mech. **23**, 384–392 (1983)
47. Lehmann, T.: Elemente der Mechanik II, Elastostatik, 2nd edn. Vieweg, Braunschweig (1984)
48. Lemaitre, J., Chaboche, J.L.: Mechanics of Solid Materials. Cambridge University Press, Cambridge (1990)
49. Liu, M.C.M., Krempl, E.: A uniaxial viscoplastic model based on total strain and overstress. J. Mech. Phys. Solids **27**, 377–391 (1979)
50. Lubliner, J.: Plasticity Theory. Macmillan Publishing Company, New York (1990)
51. Luenberger, D.G.: Linear and Nonlinear Programming. Addison-Wesley, Reading (1989)
52. Mahnken, R., Stein, E.: A unified approach for parameter identification of inelastic material models in the frame of the finite element method. Comput. Methods Appl. Mech. Eng. **136**, 225–258 (1996)
53. Mahnken, R., Stein, E.: Parameter identification for finite deformation elasto-plasticity in principal directions. Comput. Methods Appl. Mech. Eng. **147**, 17–39 (1997)
54. Malvern, L.E.: Introduction to the Mechanics of a Continuous Medium. Prentice-Hall, Englewood Cliffs (1969)
55. Nedjar, B.: On a concept of directional damage gradient in transversely isotropic materials. Int. J. Solids Struct. **88–89**, 56–67 (2016)
56. Nocedal, J., Wright, S.J.: Numerical Optimization. Springer, New York (1999)
57. Ogden, R.W.: Non-linear Elastic Deformations. Ellis Horwood, Chichester (1984)
58. Ognedal, A.S., Clausen, A.H., Polanco-Loria, M., Benallal, A., Raka, B., Hopperstad, O.S.: Experimental and numerical study on the behaviour of PVC and HDPE in biaxial tension. Mech. Mater. **54**, 18–31 (2012)
59. Press, W.H., Teukolsky, S.A., Vetterling, WTa: Numerical Recipes in Fortran, 2nd edn. Cambridge University Press, Cambridge (1992)
60. Rachev, A., Shazly, T.: A preliminary analysis of the data from an in vitro inflation-extension test can validate the assumption of arterial tissue elasticity. ASME J. Biomech. Eng. **135**(8), 084502 (2013)
61. Rauchs, G., Bardon, J., Georges, D.: Identification of the material parameters of a viscous hyperelastic constitutive law from spherical indentation tests of rubber and validation by tensile tests. Mech. Mater. **42**, 961–973 (2010)
62. Rothe, S.: Electro-thermo-mechanical modeling of field assisted sintering technology: Experiments, constitutive modeling and finite element analysis. Ph.D.-thesis, report no. 1/2015, Institute of Applied Mechanics, Clausthal University of Technology, Clausthal-Zellerfeld (2015)
63. Scheday, G.: Theorie und Numerik der Parameteridentifikation von Materialmodellen der finiten Elastizität und Inelastizität auf der Grundlage optischer Feldmessmethoden. Ph.D.-thesis, Report No. I–11 (2003), University of Stuttgart (Germany), Institute of Mechanics (2003)
64. Schittkowski, K.: Numerical Data Fitting in Dynamical Systems. Kluwer Academic Publication, Dordrecht (2002)
65. Schmaltz, S., Willner, K.: Comparison of different biaxial tests for the identification of sheet steel material parameters. Strain **40**, 389–403 (2014)

66. Schmaltz, S., Willner, K.: Material parameter identification utilizing optical full-field strain measurement and digital image correlation. J. Jpn. Soc. Exp. Mech. **13**, s120–s125 (2013)
67. Schmidt, U., Mergheim, J., Steinmann, P.: Identification of elastoplastic microscopic material parameters within a homogenization scheme. Int. J. Numer. Methods Eng. **104**, 391–407 (2015)
68. Schmidt, U., Steinmann, P., Mergheim, J.: Two-scale elastic parameter identification from noisy macroscopic data. Arch. Appl. Mech. **86**, 303–320 (2016)
69. Serban, R., Freeman, J.S.: Identification and identifiability of unknown parameters in multibody dynamic systems. Multibody Syst. Dyn. **5**, 335–350 (2001)
70. Shafiq, M., Ayyagari, R.S., Ehaab, M., Vural, M.: Multiaxial yield surface of transversely isotropic foams: Part II—experimental. J. Mech. Phys. Solids **76**, 224–236 (2015)
71. Shildip, D.U., Bhope, D.V., Khamankar, S.D.: Stress analysis of multilayer pressure vessel. J. Appl. Mech. Eng. **4**(2), 1–6 (2015)
72. Sutton, M.A., Orteu, J.J., Schreier, H.W.: Image Correlation for Shape, Motion and Deformation Measurements. Springer, New York (2009)
73. Sutton, M., Badel, P., Avril, S., Lessner, S.: Mechanical identification of hyperelastic anisotropic properties of mouse carotid arteries. In: Proulx, T. (ed.) Mechanics of Biological Systems and Materials, Proceedings of the 2011 Annual Conference on Experimental and Applied Mechanics, vol. 2, pp. 11–17. Springer, New York (2011)
74. Thielecke, F.: Parameteridentifizierung von Simulationsmodellen für das viskoplastische Verhalten von Metallen—Theorie, Numerik, Anwendung. No. 34-1998, Technische Universität Braunschweig (1997)
75. Tikhonov, A.N., Goncharsky, A.V., Stepanov, V.V., Yagola, A.G.: Numerical Methods for the Solution of Ill-posed Problems. Kluwer Academic Publishers, Dordrecht (1995)
76. Timoschenko, S.P., Goodier, J.N.: Theory of Elasticity, 3rd edn. McGraw-Hill Book Company, Singapore (1985)
77. Truesdell, C., Noll, W.: The Non-Linear Field Theories of Mechanics, Encyclopedia of Physics. Springer, Berlin (1965)
78. Twizell, E.H., Ogden, R.W.: Non-linear optimization of the material constants in Ogden's stress-deformation function for incompressible isotropic elastic materials. J. Aust. Math. Soc. Ser. B **24**, 424–434 (1983)
79. Yeh, M., Kyriakides, S.: On the collapse of inelastic thick-walled tubes under external pressure. ASME J. Energy Resour. Technol. **108**(1), 35–47 (1986)
80. Young, W., Budynas, R.: Roark's Formulas for Stress and Strain. McGraw-Hill Professional, New York (2001)